Phys. Status Solidi B **246**, No. 5, 909–928 (2009) / **DOI** 10.1002/pssb.200844401

physica status solidi b
www.pss-b.com
basic solid state physics

Feature Article

The magnetization of γ'-Fe_4N: theory vs. experiment

Eitel L. Peltzer y Blancá[1], Judith Desimoni[2], Niels E. Christensen[3], Heike Emmerich[4], and Stefaan Cottenier[*, 4, 5, 6]

[1] GEMyDE, Facultad de Ingeniería – UNLP, CCT-La Plata-IFLYSIB-CONICET, 1 y 47, 1900 La Plata, Argentina
[2] Departamento de Física, Facultad de Ciencias Exactas – UNLP, CCT-La Plata-IFLP-CONICET, C.C. Nº 67, 1900 La Plata, Argentina
[3] Department of Physics and Astronomy, University of Aarhus, Ny Munkegade, Bld. 1520, 8000 Aarhus C, Denmark
[4] Computational Materials Engineering (CME), Institute for Minerals Engineering (GHI), Center for Computational Engineering Science (CCES) & Jülich–Aachen Research Alliance (JARA), RWTH Aachen University, 52064 Aachen, Germany
[5] Instituut voor Kern- en Stralingsfysica, Katholieke Universiteit Leuven, Celestijnenlaan 200 D, 3001 Leuven, Belgium
[6] Center for Molecular Modeling, Ghent University, Proeftuinstraat 86, 9000 Ghent, Belgium

Received 10 October 2008, revised 24 December 2008, accepted 29 January 2009
Published online 19 March 2009

PACS 71.15.Mb, 71.15.Nc, 75.25.+z, 75.30.Cr, 75.50.Bb, 76.80.+y

[*] Corresponding author: e-mail stefaan.cottenier@ugent.be

By reviewing the experimental and theoretical literature on γ'-Fe_4N, and by a systematic survey of predictions by the LDA, PBE, WC, LDA + U (2×), PBE + U (2×) and B3PW91 exchange-correlation functionals, the structural, magnetic and hyperfine properties of this material as well as their pressure dependencies are interpreted. The hypothesis is put forward that γ'-Fe_4N as found in Nature is exactly at a steep transition between low-spin and high-spin behaviour. PBE + U (U = 0.4 eV) is identified as the most accurate exchange-correlation functional for this material, although it is needed to fix the magnetization at the experimental value to obtain a satisfying description. Remaining disagreement between theory and experiment is pointed out. A recent experimental claim for a giant magnetic moment in γ'-Fe_4N is discussed, and is not reproduced by our calculations. We expect that the new insight obtained in the present work can lead to a consistent *ab initio* modeling of other materials in the iron-nitrogen binary system. In an accompanying didactic section, the physics behind some common exchange-correlation functionals is outlined.

1 Introduction and motivation

Given its simple composition and crystal structure, γ'-Fe_4N displays a remarkably rich behaviour that has fascinated applied as well as basic researchers for as long as 80 years. During this period, a considerable amount of experimental as well as theoretical work has been performed. Many of these results are collected and interpreted in the present Feature Article, and supplemented with new systematic first principles calculations. By comparing the best available experimental data with a variety of theoretical descriptions, we will try to point out what is understood and what is still problematic about γ'-Fe_4N, with emphasis on structural and magnetic properties.

1.1 History and interest

The earliest interest – around 1930 – in the synthesis and study of γ'-Fe_4N was motivated by its possible application as a catalyst for the production of ammonia and for its role in the surface treatment of steels with ammonia [1]. By X-ray diffraction on powder samples, the crystal structure was readily determined to be $Pm\bar{3}m$ [1–3], a result that was much later confirmed by measurements on single crystals [4] (Fig. 1 and Section 3.1). Soon emphasis shifted to studying the basic properties of this material, which could be considered as an experimental model for expanded γ-Fe (fcc) [5]. The first magnetization study showed a magnetic moment of 8.86μ_B per unit cell at 0 K [6], which means the average

magnetic moment per Fe atom is as high as in the strong ferromagnet α-Fe (bcc). There was discussion for a while about the magnetic structure [7, 8], until neutron diffraction experiments showed that γ′-Fe_4N is a ferromagnet with a magnetic moment of $3.0\mu_B$ for the corner site (1a, here called Fe-I) and $2.0\mu_B$ on the face centered site (3b, here called Fe-II) (Fig. 1) [5]. Mössbauer experiments confirmed the value of these moments for the individual atoms [9–11]. Mössbauer and Kerr experiments showed the magnetization direction to be [001] [12–14, 135]. The Curie temperature was determined to be 761 K [6] or 767(10) K [9].

Due to its simple unit cell, γ′-Fe_4N was a suitable target for the first generation of *ab initio* methods (Table 1). A set of studies using mostly the Local Density Approximation (LDA) [15] within Density Functional Theory (DFT) [16–18] is listed in Table 1 (*note that a list of all acronyms used in this paper is given in Table 13*). All of them confirm the experimental fact [5, 9] that Fe-I has a considerably larger moment than Fe-II. The ASW method underestimates the generally accepted experimental value for the magnetic moment per unit cell by up to more than $1\mu_B$, LMTO-ASA overestimates it by $0.1–0.6\mu_B$ and FLAPW by $0.5–0.8\mu_B$. We will come back to this systematic overestimation in Section 5. From the conceptual point of view, these calculations were able to explain the physics behind the different moments on the two Fe sites in terms of the Fe–N 3d–sp hybridisation (Ref. [19], discussed in Ref. [20]).

A second wave of attention for γ′-Fe_4N followed once its potential as a material for high-density magnetic recording was pointed out [38–40]. In the following years, γ′-Fe_4N was studied as a component in various thin film devices, due to its high magnetic flux density, low coercivity, low resistance and other suitable properties [41–44, 21]. Another iron-nitride compound that came into the picture for much the same reasons was $Fe_{16}N_2$. There were several experimental claims that the average magnetic moment per Fe atom in the latter compound could reach an exceptionally large value of $3.5\mu_B$ [45–50]. As was extensively discussed by Coehoorn [27], Coey [51, 20] and Sakuma [52], these claims are not easily made consistent with other theoretical and experimental evidence at hand. The highest magnetization values were never reproduced in independent experiments, and an average moment of $2.3–2.6\mu_B$ per Fe – which is still large – is believed to be more realistic. As we will point out here, a similar discussion has recently been initiated about the "well-established" γ′-Fe_4N.

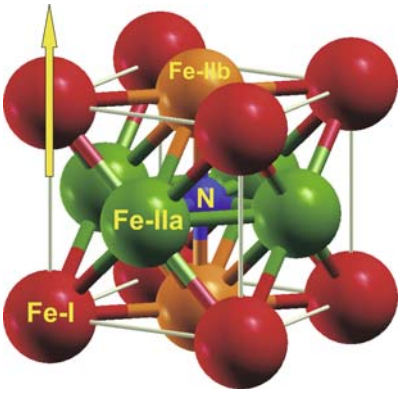

Figure 1 (online colour at: www.pss-b.com) Unit cell of ferromagnetic γ′-Fe_4N, with 3 inequivalent Fe-sites. Fe-I has a larger moment than Fe-IIa and Fe-IIb. Without magnetism, Fe-IIa and Fe-IIb are equivalent. The preferential direction of the magnetic moments (arrow) makes them inequivalent: for Fe-IIa, the four-fold rotation axis perpendicular to the local face of the cube is perpendicular to the moment, for Fe-IIb it is parallel to the moment.

During the past decade, most experimental work on γ′-Fe_4N was devoted to produce it as an epitaxial thin film [13, 37, 42, 53–64] or as a part of multilayer systems [65, 66], using different substrates and growth methods. Table 2 lists a set of synthesis methods and conditions we could find in the literature for samples for which the magnetization has been measured. Up to last year, all 12 samples from this table that were examined by conventional magnetometery at room temperature, showed a saturation magnetization between $7.6\mu_B$ and $8.7\mu_B$ per formula unit. The magnetization at low temperatures is somewhat larger ($8.9–9.2\mu_B$/f.u.). The spread in these numbers reflects experimental inaccuracies as well as differences between samples (grain size, substrate, bulk or film). In the light of this large and consistent set of data, it came as a surprise when Atiq et al. [21] reported recently a room temperature magnetization of $10.3\mu_B$ to even $11.6\mu_B$ per formula unit on well-characterized γ′-Fe_4N samples grown on several substrates. They explain this by a reduced lattice mismatch with the substrate, which is insufficient an explanation, however, as we will discuss in Section 6. This is reminiscent to the discussion about a possible giant magnetization

Stefaan Cottenier got his Ph.D. in Physics from the Katholieke Universiteit Leuven (Belgium) in 1997. He continued to work there until 2007, in the area of computational nuclear condensed matter physics. After a one-year stay at RWTH Aachen University (Germany), he is since end 2008 at the Center for Molecular Modeling of Ghent University (Belgium, molmod.ugent.be). His research work aims at combining experimental evidence with information from ab initio simulations, following the belief that one can get more insight by the combination of theory and experiment than by either of them alone. Emphasis is on problems in the context of magnetism, strong electron correlations and hyperfine interactions.

Table 1 Overview of *ab initio* calculated magnetic moments for γ′-Fe_4N. The first 16 entries are found in the literature. The next 8 entries are calculated in this work, using 8 different exchange-correlation functionals and fixing the lattice constant to the experimental one. The last 8 entries are similar, but at the equilibrium lattice constant for the corresponding functional. The columns list the exchange-correlation functional that is used, the numerical method used to solve the Kohn–Sham equations, the lattice constant at which the calculation is made ('exp' means the experimental lattice constant of 3.790 Å), the moments at the 3 magnetically inequivalent Fe sites (italics indicate cases where no spin-orbit coupling was applied and where the Fe-IIa and Fe-IIb moments are therefore necessarily identical), and the total moment per unit cell (italics indicate cases where this is a weighted sum over de individual moments only, not accounting for contributions from the region outside muffin tin spheres or from the nitrogen atom). All literature values give spin moments only, while the values obtained in this work are the sum of spin and orbital moments (see also Table 10). The last two lines give the commonly accepted experimental values for the individual moments and the total moment, as well as the recent and quite different values by Atiq et al. [21] (see also Table 2). U_1 = 0.4 eV, U_2 = 1.8 eV (see Section 4).

			magnetic moment (μ_B)					
functional	method	a_0 (Å)	Fe-I	Fe-IIa	Fe-IIb	unit cell	Ref.	year
LDA	ASW	exp	*2.98*	*1.79*	*1.79*	*8.35*	[22]	1988
LDA	LMTO-ASA	exp	*3.07*	*2.03*	*2.03*	*9.16*	[23, 24]	1991
LDA	LMTO-ASA	exp	*3.10*	*1.94*	*1.94*	*8.92*	[25, 26]	1992
LDA	LMTO-ASA	exp	*3.09*	*2.11*	*2.11*	*9.42*	[10]	1992
LDA	FLAPW	exp	*2.98*	*2.23*	*2.23*	*9.67*	[27]	1993
LDA	LMTO-ASA	exp	*3.22*	*2.01*	*2.01*	*9.25*	[28]	1994
LDA	DVM-SCC	exp	*2.97*	*2.03*	*2.03*	*9.06*	[29]	1994
LDA	LMTO-ASA	exp	*3.16*	*2.06*	*2.06*	*9.34*	[30, 31]	1996
LDA	FLAPW	exp	*2.92*	*2.14*	*2.14*	*9.34*	[32]	1999
LDA	ASW	exp	*2.91*	*1.52*	*1.52*	*7.47*	[32]	1999
LDA	FLAPW	exp	*2.73*	*1.97*	*1.97*	*8.64*	[33]	1999
LDA	FLASTO	exp	*2.98*	*2.23*	*2.23*	*9.67*	[34]	2000
LDA	FLAPW	exp	*2.92*	*2.18*	*2.18*	*9.46*	[35]	2003
PBE	FLAPW	exp	*2.90*	*2.33*	*2.33*	*9.89*	[36]	2004
PBE	LCAO	exp	*2.99*	*2.39*	*2.39*	*10.16*	[37]	2007
LDA + U [a]	TB	exp	*3.08*	*2.39*	*2.39*	*9.95*	[34]	2000
LDA	APW + lo	exp	2.91	2.17	2.21	9.72	this work	2008
PBE	APW + lo	exp	2.94	2.35	2.38	10.19	this work	2008
WC	APW + lo	exp	2.93	2.30	2.34	10.08	this work	2008
LDA + U_1	APW + lo	exp	2.94	2.32	2.36	10.18	this work	2008
LDA + U_2	APW + lo	exp	3.07	2.61	2.67	11.07	this work	2008
PBE + U_1	APW + lo	exp	2.98	2.44	2.48	10.46	this work	2008
PBE + U_2	APW + lo	exp	3.10	2.69	2.74	11.19	this work	2008
B3PW91	APW + lo	exp	3.11	2.72	2.70	11.10	this work	2008
LDA	APW + lo	3.63	2.78	1.16	1.18	6.46	this work	2008
PBE	APW + lo	3.79	2.90	2.32	2.35	10.18	this work	2008
WC	APW + lo	3.69	2.89	1.49	1.52	7.54	this work	2008
LDA + U_1	APW + lo	3.64	2.88	1.36	1.39	7.15	this work	2008
LDA + U_2	APW + lo	3.72	2.98	2.46	2.56	10.66	this work	2008
PBE + U_1	APW + lo	3.80	2.98	2.45	2.49	10.50	this work	2008
PBE + U_2	APW + lo	3.83	3.12	2.74	2.79	11.34	this work	2008
B3PW91	APW + lo	3.83	3.09	2.70	2.72	11.15	this work	2008
experiment		3.7900(6) [4]	3.0(1) [5]	2.01(4) [5]	2.01(4) [5]	8.86 [6] 11.6 [21]		1958, 1946 2008

[a] U = 1 eV – Hubbard model hamiltonian with LDA wave functions as input, no full band structure scheme.

in $Fe_{16}N_2$ (see earlier in this section), and has led us to revisit the experimental and theoretical information on γ′-Fe_4N.

At the theoretical side, it is clear from Table 1 that the majority of all *ab initio* studies on γ′-Fe_4N were performed at the LDA level of DFT. This excludes the effect of strong electron correlations in the Fe 3d orbitals. For a transition metal nitride, it is not *a priori* obvious that strong electron correlations are irrelevant, and their presence would surely enhance the total magnetic moment. For $Fe_{16}N_2$, enhanced correlations were examined [71] by the LDA + U method. The moment was indeed found to be enhanced, but the values used for U (1–4 eV) were later criticized as being unrealistically large [34]. For γ′-Fe_4N, we found only an

Table 2 Overview of different preparation methods for γ′-Fe_4N and their relation to the magnetic moment per formula unit (μ/f.u.) determined at the temperature indicated in the second column. The first group contains samples where the magnetic moment was measured at low temperatures. The second group contains coarse powders and thick films at room temperature, whereas nanosystems (powders and films) at room temperature are collected in the third group. The final group reports the recent measurements by Atiq et al. [21] where the total moment is considerably larger than in any previous study.

μ/f.u. (μ_B)	T (K)	sample type	substrate	mismatch	method	preparation temperature	annealing	Ref.	year
8.86	0	powder	–	–	NH_3/H_2 flow	550 °C	no	[6]	1946
9.1(2)	0	powder	–	–	NH_3/H_2 flow	500 °C	no	[9]	1962
8.8(2)	4.2	powder	–	–	NH_3/H_2 flow	500 °C	no	[67]	1960
8.9(2)	4.2	powder	–	–	NH_3/H_2 flow	500 °C	no	[11]	1994
8.7	4.5	powder	–	–	NH_3/H_2 flow	450 °C	no	[68]	1996
9.22	5	µm-film	Si or kapton	–	rf-MS	RT	no	[53]	1994
8.59	0	thin film (55 nm grains)	Si(100)	1%	dc-MS	250 °C	no	[69]	2009
9.0[a]	RT	powder	–	–	NH_3/H_2 flow	?	?	[5]	1958
8.4(2)	300	powder	–	–	NH_3/H_2 flow	500 °C	no	[9]	1962
7.69	300	µm-film	Si or kapton	–	rf-MS	RT	no	[53]	1994
8.2	RT	thick film	–	–	dc-MS	?	no	[65]	1997
8.0(1)	RT	powder	–	–	NH_3/H_2 flow	500 °C	no	[59]	2000
8.71	RT	film (60–100 nm)	Ag(100)/Si(100)	8%	dc-MS	100 °C	no	[56]	1996
7.80	298	nanopowder (22 nm)	–	–	NH_3/H_2 flow	500 °C	no	[70]	1998
7.59	RT	granular film (40–60 nm grains)	NaCl(100)	5%	dc-MS	150 °C	no	[64]	2006
7.74	RT	film	MgO(100)	10%	CVD	600 °C	no	[61]	2001
8.17	300	nm-film (60 nm)	$SrTiO_3$(100)	3%	sputter	350–450 °C	no	[42]	2003
8.35	RT	nm-film (5-200 nm)	MgO(100)	10%	sputter	600 °C	no	[63]	2003
8.4	RT	nm-film (36 nm)	MgO(100)	10%	MBE	400 °C	no	[13]	2004
7.78	RT	thin film (55 nm grains)	Si(100)	1%	dc-MS	250 °C	no	[69]	2009
10.3(1)	RT	nm-film (55 nm)	MgO(100)	11%	dc-MS	450 °C	30 min @ 450 °C	[21]	2008
11.0(1)	RT	nm-film (55 nm)	$SrTiO_3$(100)	3%	dc-MS	450 °C	30 min @ 450 °C	[21]	2008
11.6(1)	RT	nm-film (55 nm)	$LaAlO_3$(100)	0%	dc-MS	450 °C	30 min @ 450 °C	[21]	2008

[a] obtained by a sum over individual moments.

LDA + U study in the context of a model hamiltonian, not within a first principles scheme [34].

1.2 Aim of this paper The present paper has several aims. We want to bring together in one paper as much as possible experimental and theoretical facts about γ′-Fe_4N that are now spread over the literature, and assess their quality and reliability (Sections 1 and 3). In other words: what do we know about Fe_4N, and how do we know it? This information will then be matched against a systematic series of *ab initio* calculations at various levels of sophistication (Section 4). From this comparison, the method that currently provides the best description of γ′-Fe_4N will be singled out (Section 5), and remaining disagreement between theory and experiment will be indicated. Experimental and theoretical issues that deserve further attention will be discussed: the exceptionally large magnetization recently observed by Atiq et al. (Section 6), the systematic overestimation of the saturation magnetization by any *ab initio* method and the possible difference in hyperfine fields for Fe-IIa and Fe-IIb (Sections 5 and 7).

It happens increasingly often in *ab initio* studies in condensed matter physics that calculations with different exchange-correlation functionals are made and interpreted (e.g. Ref. [72, 73]). In chemistry, such an approach is being used more routinely (e.g. Ref. [74]). This might easily give the impression of 'forcing the theory until it matches any experiment'. Another goal of this Feature Article is therefore to point out for a non-theoretical audience what are the relations between some of the most common approximations within DFT, and when it is justified to use them. Section 2 is devoted to this – it can be read independently from the rest of the paper, and readers mainly interested in γ′-Fe_4N can safely skip it if they wish. Where appropriate, Section 2 refers to γ′-Fe_4N as an illustration.

2. XC-functionals and beyond

2.1 One theory, many flavours When the first wave of applications of the Density Functional Theory (DFT) [18] started to flood the condensed matter physics community about 20 years ago, the conceptual framework was very simple. There was the formal description of DFT as given by Hohenberg, Kohn and Sham [16, 17] another 20 years before – not suited for practical calculations as the magic 'true exchange-correlation functional' was not known. And there was a simple and unexpectedly successful approximation to this functional: the Local Density Approximation (LDA). The limited computer power available around 1990 forced scientists to apply more numerical approximations than they might have liked, but at least there was not much debate on the heart of the method: a prediction based on LDA could agree or could not agree with Nature, but it was 'the' theoretical prediction. Today, there is much more computer power around, and in many cases we can afford to go to full numerical accuracy. If differences between calculated properties and experimental observations appear, then the approximation for the exchange-correlation functional itself has to blamed (provided the interpretation of the experimental observations is correct!). The increase of numerical precision therefore went along with the appearance of new ways to approximate the exchange correlation-functional better and to cure in this way the imperfections of LDA. Neither as LDA does, these functionals work for all possible situations. Choosing the most justified functional has become an important step in a 'first' principles study – mind the *contradictio in terminis*. This is well-known by theoreticians who perform DFT calculations, but it is the experience of the authors that this point causes discomfort in the experimental community where DFT is applied increasingly more often as well. An experimentalist who turns to a DFT computer code to illuminate a specific problem gets several answers instead of one. How to make sense of that?

In this section – which can be skipped by readers interested mostly in γ'-Fe_4N – we focus on five important choices for the exchange-correlation functional, with their *ad hoc* fixes where appropriate, and point out their general properties. The audience we have in mind for this more didactic section are in the first place researchers outside the first principles community, who want to get in a few paragraphs the basic information needed to read research papers containing *ab initio* results. For a more complete and a more technical discussion of the same topic, we refer to the recent review by Hafner [75], and the many references therein.

2.2 XC-functionals and beyond: what and why As in the majority of present-day first principles studies, we work in the frame-work of Density Functional Theory. DFT is a formally exact method, that can describe all properties of atoms, molecules and solid with absolute correctness (Table 3, first row). This ideal version of DFT needs a universal functional of the electron density, the so-called exchange-correlation (XC) functional. DFT tells us only that this functional exists, but does not specify its mathematical formula. A specific choice for this functional can be validated only by comparing how the observable properties it predicts compare with experiment. Sometimes a systematic deviation appears between prediction and experiment, for well-defined classes of materials. That can trigger the introduction of 'patches' to the XC-functional, either fully *ad hoc* or based on physical considerations. The calculations in this work use several choices for the XC-functional and for such 'patches' (Table 3, second row). We will list here in general terms the major properties of these and other possible choices:

Table 3 Hierarchy of approximations in going from the formal and exact version of DFT (Level 1) to a tool for practical calculations (Level 3). The physics is approximated at the second level, whereas the numerical approximations at the third level are of a technical nature. Sufficiently fast computers allow to go to full numerical accuracy in Level 3, such that only the second level remains as a source for possible disagreement with Nature.

Level 1	formal DFT	not available in practice
Level 2	approximate XC functionals	LDA, GGA, OP, LDA + *U*, hybrids, . . .
Level 3	numerical approximations	basis set size, *k*-mesh, selfconsistency, . . .

– *Local Density Approximation* (*LDA*). This is the oldest and simplest XC-functional, suggested already by Kohn and Sham in 1965 [17]. It approximates the exchange-correlation energy of the entire solid as an integral of the exchange-correlation energy at any point in the solid, where the latter is assumed to be given by the exchange-correlation energy of a homogeneous electron gas with the same overall density as the density at the given point. An analytic expression for this has been given by Perdew and Wang [15], based on energies for the homogeneous electron gas that were obtained by Ceperly and Alder [76] using quantum Monte Carlo calculations. There is basically only one form for LDA. Given the crudeness of this approximation, LDA has been unexpectedly successful. Up to the mid-nineties it was the only XC-functional in use. It has two major disadvantages: it makes atomic bonds too strong, resulting in too small lattice constants ('overbinding' – see Table 4 for γ'-Fe_4N). And it makes localized electrons itinerant, leading to a qualitatively wrong description of strongly correlated materials.

– *Generalized Gradient Approximation* (*GGA*). This functional extends the idea behind LDA. In order to account for the fact that the density in a real solid is not uniform as in the homogeneous electron gas, it determines the contribution to the exchange-correlation energy at a given point not only by the density at that point, but by taking into account the gradient of the density at that point as well. There are many ways to express this idea, ranging from semi-empirical GGA's that are fitted to reproduce specific systems to GGA's that are based on fundamental quantities

only, just as LDA. The version due to Perdew, Burke and Ernzerhof (PBE) [77] is a popular non-empirical GGA, and was during the past decade perhaps the most commonly used functional. Recently Wu and Cohen (WC) [78] proposed a slightly different GGA, which promises to perform even better than PBE for some classes of materials. GGA's tend to correct the overbinding of LDA (and sometimes underbind), with WC giving a value often intermediate between LDA and PBE [73] (see Table 4 for an illustration on γ′-Fe_4N). They have a tendency to make magnetic effects too strong, and are just as LDA not suitable for strongly correlated materials. GGA's tend to describe surface properties less well than LDA does, especially for elements heavier than the 3d series [73, 79].

– *Orbital Polarization* (*OP*). There is a philosophical difference between a 'first principles method' and a parameter-free method. Strictly spoken, the latter means one cannot tune any parameter in the method, while the former indicates a method that is directly derived from the fundamental equations of quantum mechanics. A first principles method is *a fortiori* parameter-free. As DFT in its LDA or GGA formulation contains a XC-functional that corresponds to a specific choice of approximation, it is not really a first principles method. As long as the expression for the XC-functional is kept unaltered, the method is still parameter-free, however. It is tempting to introduce a tuneable parameter ('a patch') in the method in order to fix *ad hoc* shortcomings of the XC-functional. This is what happens in the three methods that now will be described. As long as this tuneable parameter is there for physical reasons, and as long as it is not misused for blind fitting, this is a useful approach that can provide insight in the problem at hand. The Orbital Polarization correction addresses the problem that the orbital moment as given by LDA or GGA is often too small by a factor of 2 or more [80–82] (see Section 5.3 for γ′-Fe_4N). The cure can be as simple as rescaling the orbital moment by such a factor [83, 84]. This will bring other properties that indirectly depend on the orbital moment in better agreement with experiment as well.

– *LDA + U*. This method is meant to describe strongly correlated systems better than LDA and GGA do. LDA renders electrons as itinerant that are localized in Nature, because it too much penalizes electrons of unlike spin when they appear in each other's neighbourhood (i.e. the LDA exchange energy is incorrect). In Nature, each electron carries an 'exchange-correlation hole' around it – a zone that is depleted of other electrons. LDA and GGA do not describe this hole very accurately. Therefore, a tuneable parameter U is introduced, with the dimensions of energy. This extra energy is removed from the system when electrons of unlike spin are closely together. As a result, the tendency to localize electrons at a given site increases. Classes of materials where LDA + U is helpful are lanthanide compounds (4f electrons are strongly localized) and transition metal oxides (e.g. 3d electrons are reasonably localized in such materials). The question "*which U did you use and why*" inevitably arises when this method is applied – in Section 4 we address this question for γ′-Fe_4N. The name LDA + U is sometimes used as the general name to indicate this class of methods, together with more specific indications as GGA + U or PBE + U (e.g. Ref. [85]).

Table 4 Basic structural properties of γ′-Fe_4N: lattice constant (a_0), bulk modulus at equilibrium (B_0) and pressure derivative of the bulk modulus (B_0'). The calculated data are obtained from a Birch–Murnaghan fit [97] in the volume range ±10% around the equilibrium, unless this volume range contains the steep feature in the magnetization curve (Fig. 4 and Table 12) – in the latter cases, a smaller volume range was used. The experimental data are obtained at room temperature, which makes them less ideal to compare with *ab initio* calculations. $U_1 = 0.4$ eV, $U_2 = 1.8$ eV (Section 4).

method	a_0 (Å)	B_0 (GPa)	B_0'
LDA	3.636	272	5.3
PBE	3.789	200	4.6
WC	3.691	211	6.4
LDA + U_1	3.644	272	4.7
LDA + U_2	3.718	234	4.5
PBE + U_1	3.797	195	4.8
PBE + U_2	3.826	184	4.4
B3PW91	3.825	196	6.6
exp (RT) [95]	3.798(1)	141	9.6
[96]		196(4)	1[a]

[a] The linear relation between volume and pressure as shown by the experimental data in Ref. [96] implies $B_0' = 1$.

– *Hybrid XC-functionals*. While LDA + U has a history of more than a decade now, hybrid functionals are of a more recent date in condensed matter physics. The idea is to 'borrow' the exchange energy that is missing in LDA or GGA from a method that gives exchange exactly: the Hartree–Fock method. This is not as easy as it might seem, for two reasons. First, LDA already contains some exchange. But one does not know how much, and therefore it remains a guess how much missing exchange has to be added. Second, one of the reasons why LDA performs so well is a lucky balancing of errors in its exchange and correlation parts. Fiddling with the exchange part only might disturb this balance, and lead to a worse rather than a better description. In practice, the fraction of Hartree–Fock exchange that needs to be added is fitted against a database of test compounds, and subsequently kept fixed. This is the idea behind the B3LYP [86, 87] and B3PW91 [86] hybrid functionals, which contain 20% Hartree–Fock exchange and which are heavily used in chemistry for DFT on large molecules. There are indications, however, that in solids the amount of Hartree–Fock exchange needs to be larger [88, 89]. The large scale application of hybrid functionals in condensed matter physics has only just started [72, 85, 88–93] and much more results obtained with such functionals are expected in the near future.

There is much, much more to say on this issue, but then this section would not any longer be a short overview with the most basic information. Topics that we did not

touch are e.g. meta-GGA's, Exact Exchange and methods that go beyond the DFT framework as GW and Dynamical Mean Field Theory. For these 'more advanced' topics we refer to the specialized literature (e.g. [75] and references therein).

The preceding overview shows that before performing an *ab initio* study, it really matters to think about which level of theory is appropriate. This choice can be guided by the physics behind the construction of the functionals (e.g. strongly correlated materials are tackled by LDA + U rather than by LDA) and/or by experience gathered in the literature (see e.g. [73]). As far as γ′-Fe_4N is concerned, nearly all calculations published so far were done at the LDA or PBE level (Table 1). This was mainly by lack of alternatives at those times, as many of these studies were done before functionals as LDA + U became routinely available. Indeed, just as the transition metal oxides, transition metal nitrides can display strong electron correlations, and a functional suitable for this type of problems should be used in the first place. It has been suggested at least twice [51, 52] to examine γ′-Fe_4N with LDA + U. This was done in Ref. [34] in the frame of a model hamiltonian, and in Ref. [71] at the *ab initio* level for the related compound $Fe_{16}N_2$ – in the latter case with a manifestly too large value for the parameter U, though. Ref. [32] pointed to the need to examine γ′-Fe_4N with different exchange-correlation functionals, which is what will be done systematically in the present paper.

2.3 Numerical solution methods After having made a choice for the exchange-correlation functional, one ends up with a system of differential equations that needs to be solved numerically (third row in Table 3). Another list of numerical approximations is now needed to obtain the solutions. This gives rise to a manifold of numerical methods, each of them containing more (ASW, LMTO-ASA, LCAO, . . .) or less (FLAPW, FLMTO, APW+lo, . . .) numerical approximations. With the computers that are nowadays routinely available, it is often affordable to make these numerical approximations that good that they are indistinguishable from an exact solution. This is therefore a fundamentally different kind of approximation than the choice of the exchange-correlation functional, where more computer power does not help to make the approximations better. We mention this topic here for completeness, but it is not the goal of this paper to elaborate on issues as basis set types, special k-points, series expansions, fourier transforms, etc. Many details about this can be found for instance in Ref. [94]. The choices for the numerical approximations that are made in the present work, can be found in Section 4.

3. Facts about γ′-Fe_4N

3.1 Structural information The basic information on the crystal structure of γ′-Fe_4N is summarized in Fig. 1 and Table 4. The unit cell can be described as a fcc Fe cube with one nitrogen atom at the body center. The (chemical) space group is $Pm\bar{3}m$ (nr. 221), with one Fe-atom (Fe-I) at a cubic m3m site (1a) and 3 Fe atoms (Fe-II) at a tetragonal 4/mmm site (3c). Nitrogen is at a cubic $m\bar{3}m$ site (1b). The experimental lattice constant at room temperature is 3.7900(6) Å (Ref. [4], other reported room temperature bulk lattice constants are all close to this: 3.795 Å [3, 8] and 3.798 Å [95]). We found no low-temperature lattice constant data. We are aware of two measurements of the bulk modulus at room temperature, which do not really agree with each other: 141 GPa [95] and 196(4) GPa [96]. Both were determined by X-ray diffraction at a synchrotron, with the sample in a diamond anvil cell. The value of 141 GPa looks to be more reliable (more data points, larger pressure range examined, several independent diffraction peaks taken into account, fitted with an equation of state). The magnetic properties of γ′-Fe_4N were discussed in Section 1. The presence of ferromagnetic moments along the 001-direction [12–14, 135] breaks the chemical symmetry. The space group of the *magnetic* unit cell is lowered to P4/mmm (nr. 123). The reduced point group for Fe-I and N is 4/mmm (1a and 1d). The Fe-II site is split in Fe-IIa with point group mmm and multiplicity 2 (2e), and Fe-IIb with point group 4/mmm and multiplicity 1 (1c).

3.2 Mössbauer and NMR experiments Mössbauer spectroscopy is able to infer local information in solids by detecting magnetic hyperfine fields and electric-field gradients (EFG) at the nuclei of suitable isotopes. The element Fe has an isotope (^{57}Fe) with the most favorable nuclear parameters for Mössbauer spectroscopy, which explains why γ′-Fe_4N has been extensively studied by this method. The three inequivalent Fe sites in the magnetic space group P4/mmm are by symmetry reasons characterized by different combinations of hyperfine fields and EFG's. Fe-I feels basically a magnetic hyperfine field only: the non-cubic symmetry of this site, which in principle would allow for the existence of an EFG, is due to the presence of the ferromagnetic moment only, while it is mainly the chemical symmetry which determines the EFG. Indeed, the maximal value we have calculated for the principal component V_{zz} of the EFG tensor at this site is as low as 0.05×10^{21} V/m^2. Fe-IIa and Fe-IIb feel a combined magnetic/electric hyperfine interaction. The EFG tensor has at both sites its principal z-axis perpendicular to the local face of the unit cell, such that it makes an angle $\theta = 90°$ with the hyperfine field along [001] for Fe-IIa, and an angle $\theta = 0°$ for Fe-IIb. In order to calculate the combined magnetic/electric hyperfine splitting, the magnetic hyperfine field and the EFG tensor should be expressed in the same coordinate system. The principal component V_{zz} of the EFG tensor is transformed as follows to the axis system that has its z-axis parallel to the magnetic hyperfine field:

$$V'_{zz} = V_{zz} \frac{3\cos^2\theta - 1}{2}. \quad (1)$$

Table 5 Overview of Mössbauer and NMR experiments in Fe_4N: temperature T (K) at which the measurement was performed, if measured: the saturation magnetization μ (Bohr magneton per formula unit) at the same temperature, the magnetic hyperfine field B_{hf} (T) for the three Fe sites, the isomer shift δ (mm/s) relative to α-Fe for the three Fe sites, the quadrupole interaction ε (mm/s) for the two non-cubic Fe-sites, and the principal component V_{zz} (10^{21} V/m^2) of the EFG tensor (deduced from the measured ε by Eq. (2), using $\theta_{IIa} = 90°$ and $\theta_{IIb} = 0°$). Magnetization data are given only if they are measured on the same kind of sample as used for the Mössbauer experiments. When magnetization information was available only at low temperature, a factor 0.88 was used to convert it to room temperature (this is an average of the experimental values of 0.92 [9] and 0.83 [53], and close to a very recent and apparently accurate value of 0.91 [69]). Refs. [101] and [68] use NMR, the others use Mössbauer spectroscopy. The sign of B_{hf} is usually not measured, but a negative sign is used throughout the table, as suggested by all available *ab initio* calculations (Table 6). Refs. [102] and [96] gave their isomer shift values with respect to CoRh – we converted them to α-Fe for consistency. Ref. [53] does not specify the reference for the isomer shift, but the values suggest it was CoRh too. In some papers, definitions of ε are used that are one half of ours – the values have been converted accordingly. This table extends previous tabulations in Refs. [14, 51, 99], of whom we have not included a few Mössbauer studies that gave only incomplete information. Data that we consider to be unreliable, are put in italics.

T (K)	μ/f.u.	B_{hf}-I	B_{hf}-IIa	B_{hf}-IIb	δ-I	δ-IIa	δ-IIb	ε-IIa	ε-IIb	V_{zz}^{IIa}	V_{zz}^{IIb}	Ref.	year
1.3	8.71	–36.9	–23.5	–23.5	–	–	–	–	–	–	–	[68]	1996
4.2	–	–36.9	–23.6	–23.8	0.38	0.42	0.42	0.27	–0.54	–3.2	–3.2	[102]	1994
4.2	–	–36.9	–23.4	–23.4	–	–	–	–	–	–	–	[101]	1994
4.2	–	–37.0	–23.7	–23.7	*0.26*	*0.32*	*0.32*	0.22	–0.47	–2.6	–2.8	[96][a]	1995
5	–	–37.0	–23.6	–23.5	0.39	0.46	0.45	0.24	–0.52	–2.9	–3.1	[104]	1986
7	9.22	–36.9	–23.7	–23.4	0.36	0.45	0.45	0.22	–0.41	–2.6	–2.5	[53]	1994
15	8.9(2)	–36.6	–23.5	–23.6	0.40	0.46	0.46	0.22	–0.45	–2.6	–2.7	[11]	1994
RT	8.4(2)	*–34.5*	*–21.5*	*–21.5*	*0.30*	*0.45*	*0.45*	–	–	–	–	[9][b]	1962
RT	–					0.30	0.30	0.21	–0.43	–2.6	–2.6	[105][a]	1970
RT	–	–34.1	–21.5	–21.9	0.24	0.30	0.32	0.22	–0.43	–2.6	–2.6	[12]	1971
RT	–	*–34.1*	*–21.7*	*–21.7*	*0.25*	*0.31*	*0.31*	*0.32*	*–0.48*	*–3.8*	*–2.9*	[106][d]	1991
295	–	–34.1	–21.8	–21.6	0.24	0.29	0.29	0.27	–0.54	–3.2	–3.2	[102]	1994
293	7.8(2)	–33.9	–21.4	–21.7	0.25	0.32	0.32	0.19	–0.40	–2.3	–2.4	[11]	1994
300	7.69	–34.0	–21.7	–21.6	0.23	0.29	0.26	0.16	–0.29	–2.0	–1.7	[53]	1994
300	–	–34.3	–21.9	–21.9	0.24	0.31	0.31	–	–	–	–	[107, 108]	1995
298	7.80	–34.4	–21.8	–22.0	0.23	0.30	0.30	0.19	–0.37	–2.3	–2.2	[70]	1998
RT	–	–34.0	–21.6	–21.9	0.20	0.27	0.27	0.20	–0.42	–2.4	–2.5	[109]	1998
RT	–	*–34.0*	*–21.8*	*–21.6*	*0.23*	*0.31*	*0.30*	*–0.20*	*0.09*	*2.4*	*0.5*	[99][e]	2001
RT	–	*–37.7*	*–23.7*	*–18.7*	*0.11*	*0.10*	*0.04*	*–0.04*	*–0.04*	*0.5*	*–0.2*	[99][e]	2001
RT	–	–34.2	–21.8	–21.8	0.23	0.30	0.30	–	–	–	–	[110]	2001
RT	–	–33.8	–21.6	–21.9	0.25	0.30	0.29	0.22	–0.37	–2.6	–2.2	[111]	2003
300	8.4	–34.1	–21.7	–21.9	0.22	0.29	0.29	0.24	–0.45	–2.9	–2.7	[13]	2004
RT	–	–33.9	–21.5	–21.7	0.24	0.31	0.31	0.19	–0.38	–2.3	–2.3	[14]	2007
823	–	0.0	0.0	0.0	–0.17	–0.08	–0.08	0.26	–0.53	–3.2	–3.2	[14]	2007

Comments:
[a] Isomer shift at odds with other data, no obvious reason. [b] Somewhat unreliable values because no EFG was taken into account in the fit. [c] Refitting of data from Ref. [103], with for the first time a correct treatment of the EFG. [d] Not clear from the paper which convention for ε is used. Moreover, the expected ratio of –2 between ε-IIa and ε-IIb is not present. [e] Unreliable analysis because the sample is a mixture of different phases.

The quadrupole splitting Δ_Q in this axis system is then

$$\Delta_Q = \frac{eQV'_{zz}}{2} = \frac{eQV_{zz}}{2}\,\frac{3\cos^2\theta - 1}{2}, \qquad (2)$$

Q is the nuclear quadrupole moment of the relevant Mössbauer nuclear level ($Q = 0.16$ b for ^{57}Fe [98]). The quadrupole splitting Δ_Q has units of energy. What is detected experimentally is the related quantity ε, which has units of speed:

$$\varepsilon = \frac{c}{E_0}\,\Delta_Q\,. \qquad (3)$$

Here c is the speed of light in vacuum, and E_0 is the energy of the Mössbauer transition (14.4 keV for ^{57}Fe). Note that sometimes another convention is used for ε, with values that are half as large as the one we use here. This has caused some confusion in the Fe_4N literature, where e.g. in Ref. [32] a calculated EFG is found to be 'in excellent agreement with experiment', although it was actually a factor 2 off. Similarly, in Ref. [14] bad samples are blamed for the large spread in ε-values reported in the literature, while most of that spread is explained by different conventions for ε. In Table 5, all ε-values were converted to the same convention.

Another quantity that is obtained from a Mössbauer experiment is the isomer shift δ for each site. The three

Table 6 Review of calculated values found in the literature for the magnetic hyperfine field B_{hf} (Tesla) and EFG (ε (mm/s) or V_{zz} (10^{21} V/m^2)) at the Fe-sites in Fe_4N, as well as new results contributed in this work. For comparison, the calculated saturation magnetization μ (μ_B per formula unit) is given as well. The hyperfine fields found in the literature contain the Fermi contact term only, while our calculations are the sum of the contact term, the orbital field and the spin dipolar field (see also Table 11). The literature values are for the experimental lattice constant, unless when marked differently in the first column. The new results are for the experimental lattice constant (2nd block) and for the theoretical lattice constant of each functional (3rd block). The last line gives the best low-temperature experimental values for comparison (interpreted average from Table 5).

functional	method	μ/f.u.	B_{hf}-I	B_{hf}-IIa	B_{hf}-IIb	ε-IIa	ε-IIb	V_{zz}^{IIa}	V_{zz}^{IIb}	Ref.	year
LDA	LMTO-ASA	8.37	–30.0	–20.4	–	–	–	–	–	[22]	1988
LDA	LMTO-ASA	9.42	–32.8	–24.5	–24.5	–	–	–	–	[10]	1992
LDA	LMTO-ASA	8.92	–32.8	–24.2	–24.2	–	–	–	–	[25, 26]	1992
LDA	FLAPW	9.67	–36.3	–21.7	–21.7	–	–	–	–	[27]	1993
LDA	ASW	–	–	–	–	0.29	–0.58	–3.48	–3.48	[102]	1994
LDA	LMTO-ASA	9.25	–36.0	–24.7	–24.7	–	–	–	–	[51]	1994
LDA	DVM-SCC	9.06	–33.3	–26.7	–26.7	–	–	–	–	[29]	1994
LDA	LMTO-ASA	9.34	–43.7	–28.1	–28.1	–	–	–	–	[30, 31]	1994
LDA	ASW	7.47	–27.3	–18.5	–18.5	–	–	–	–	[32]	1999
LDA (theo)	FLAPW	–	–	–	–	0.12	–0.23	–1.4	–1.4	[32]	1999
PBE	FLAPW	–	–	–	–	0.24	–0.50	–3.0	–3.0	[112]	2001
PBE	FLAPW	9.89	–39.3	–24.4	–24.4	0.23	–0.46	–2.8	–2.8	[36]	2004
LDA (exp)	APW + lo	9.72	–32.6	–17.3	–21.1	0.16	–0.33	–1.97	–1.96	this work	2008
PBE (exp)	APW + lo	10.19	–36.0	–19.2	–22.2	0.24	–0.47	–2.84	–2.83	this work	2008
WC (exp)	APW + lo	10.08	–33.8	–17.9	–21.3	0.21	–0.42	–2.51	–2.50	this work	2008
LDA + U_1 (exp)	APW + lo	10.18	–36.4	–18.3	–21.2	0.23	–0.46	–2.79	–2.77	this work	2008
LDA + U_2 (exp)	APW + lo	11.07	–43.3	–20.0	–20.3	0.36	–0.71	–4.36	–4.25	this work	2008
PBE + U_1 (exp)	APW + lo	10.46	–39.1	–20.3	–22.5	0.28	–0.56	–3.36	–3.35	this work	2008
PBE + U_2 (exp)	APW + lo	11.19	–45.4	–21.8	–21.8	0.38	–0.74	–4.54	–4.42	this work	2008
B3PW91 (exp)	APW + lo	11.10	–54.3	–32.5	–34.4	0.31	–0.63	–3.77	–3.79	this work	2008
LDA (theo)	APW + lo	6.46	–22.8	–15.9	–22.8	0.08	–0.16	–0.94	–0.96	this work	2008
PBE (theo)	APW + lo	10.18	–36.2	–19.3	–22.3	0.24	–0.47	–2.87	–2.85	this work	2008
WC (theo)	APW + lo	7.54	–24.8	–18.5	–25.1	0.06	–0.12	–0.71	–0.71	this work	2008
LDA + U_1 (theo)	APW + lo	7.15	–26.0	–17.6	–24.8	0.07	–0.15	–0.86	–0.88	this work	2008
LDA + U_2 (theo)	APW + lo	10.66	–42.7	–20.2	–21.5	0.38	–0.74	–4.52	–4.47	this work	2008
PBE + U_1 (theo)	APW + lo	10.50	–39.4	–20.1	–22.3	0.28	–0.56	–3.40	–3.38	this work	2008
PBE + U_2 (theo)	APW + lo	11.34	–45.9	–21.5	–21.1	0.36	–0.69	–4.30	–4.14	this work	2008
B3PW91 (theo)	APW + lo	11.15	–54.6	–32.9	–34.2	0.27	–0.54	–3.22	–3.22	this work	2008
experiment		9.0	–36.9	–23.6	–23.6	0.22	–0.45	–2.7	–2.7	Table 5	

quantities B_{hf}, ε and δ provide an experimental fingerprint for each of the three Fe sites in γ'-Fe_4N. They can be used to assess the quality of *ab initio* calculations, and are indirectly related to the saturation magnetization (see Section 5).

Table 5 gives an overview of 24 Mössbauer and NMR experiments we found in the literature, grouped according to measurement temperature (NMR can detect magnetic hyperfine fields, but not EFG's or isomer shifts). In spite of the different ways in which the γ'-Fe_4N samples have been prepared (see also Table 2), the main features of all these independent Mössbauer experiments mostly agree. This gives confidence they all examined the same material. The only two samples that show drastically deviating results are those from Ref. [99], produced by spark erosion and by plasma nitriding – these samples contained several phases, which made it hard to extract reliable parameters for γ'-Fe_4N. The low-temperature hyperfine field for Fe-I (–36.9 T near 0 K, average over the reliable low-temperature values from Table 5) is larger than for Fe-IIa and Fe-IIb (average –23.6 T near 0 K), and is 3 T (Fe-I) or 2 T (Fe-II) lower at room temperature. No values between room temperature and the Curie temperature seem to be known. The isomer shift for Fe-I (average 0.38 mm/s near 0 K) is somewhat smaller than for Fe-II (average 0.44 mm/s near 0 K) and drops by about 35% at room temperature (averages: Fe-I = 0.23 mm/s, Fe-II = 0.30 mm/s). This decreasing trend is continued at the highest measured temperature [14] of 823 K (Fe-I: –0.17 mm/s, Fe-II: –0.08 mm/s). If the measured ε-values are converted to V_{zz} (which does not depend on the angle θ with the hyperfine field, and which is the quantity that can be determined by *ab initio* calculations), then nearly identical V_{zz} values are found for Fe-IIa and Fe-IIb. Their value is about -2.7×10^{21} V/m^2 at low temperature, and is 5–10% smaller in magnitude at room temperature. There is one recent

measurement known [14] where γ′-Fe_4N was studied above its Curie temperature. It is rather surprising to observe that at this temperature the EFG becomes larger again: usually the EFG decreases with increasing temperature, due to lattice expansion and the effect of phonons [100].

For all samples where this information was available, Table 5 mentions the saturation magnetization as well (at the same temperature as the Mössbauer measurement, see caption). At low temperatures, the spread in the measured saturation magnetization is $0.4\mu_B$/f.u. (nearly 5% relative spread), at room temperature it is $0.5\mu_B$/f.u. The spread in the magnetic hyperfine fields is much smaller (only 0.4 T or 1%, for all entries that are qualified as 'reliable' and that are therefore not in italics in Table 5). This difference in relative accuracy is probably due to large incertainties in density and/or thickness determination of the sample that is needed to obtain the saturation magnetization. It suggests that magnetic hyperfine fields are a more reliable quantity for characterizing the magnetic state of γ′-Fe_4N.

Many researchers have reported *ab initio* calculated values for the Fermi contact contribution to the magnetic hyperfine field. For transition metals, this is usually by far the dominant contribution to the hyperfine field. The other contributions – the orbital hyperfine field and the spin dipolar hyperfine field – give corrections below ≈10%, and were often neglected in early calculations. Table 6 lists those calculated contact fields, as well as 2 cases where the EFG was calculated. The main features of the experimental values in Table 5 are reproduced. New results for 8 different exchange-correlation functionals are given in this table as well. In contrast to previous work, they take spin–orbit coupling into account and do contain the orbital and spin dipolar contributions – see Section 5 for a discussion of those results.

3.3 Pressure dependence Part of the fundamental interest in γ′-Fe_4N stems from the fact that it serves as a model for expanded γ-Fe (fcc). When applying pressure to γ′-Fe_4N, the volume per atom can be driven towards the value for γ-Fe, which allows interesting comparisons. These considerations have triggered several experimental [95, 101, 107, 108, 113] and theoretical [30–32, 114] studies of compressed γ′-Fe_4N. Tables 7, 8 and 9 show the available data for the pressure dependence of the saturation magnetization [101] and the hyperfine fields at Fe-I and Fe-II [96, 101] at 4.2 K (the pressure dependence of hyperfine fields at room temperature is measured as well [107, 108] but not reported here as low temperature data are more suitable for a clean comparison with theory). Previous theoretical studies that considered the pressure dependence of the Fermi contact contribution to the hyperfine field only [30–32], were able to reproduce these trends qualitatively. It was initially expected that different degrees of electron localization at the Fe-I and Fe-II sites would lead to drastically different pressure dependencies for the hyperfine fields, which was not observed in the experiments. Mohn and Matar [32] pointed out that this was

Table 7 Pressure dependence of the saturation magnetization of γ′-Fe_4N (experiment and theory). $U_1 = 0.4$ eV, $U_2 = 1.8$ eV (Section 4).

$\frac{\partial \ln \sigma_0}{\partial p}$ (GPa^{-1})	pressure range (GPa)	T (K)	Ref.
–0.036(3)	0–0.9	4.2	[101]
		method	
–0.005		LDA	this work
–0.004		PBE	this work
–0.009		WC	this work
–0.007		LDA + U_1	this work
–0.002		LDA + U_2	this work
–0.003		PBE + U_1	this work
–0.002		PBE + U_2	this work
–0.001		B3PW91	this work

Table 8 Pressure dependence of the magnetic hyperfine field on Fe-I in γ′-Fe_4N (experiment and theory). $U_1 = 0.4$ eV, $U_2 = 1.8$ eV (Section 4).

$\frac{\partial \ln B_I}{\partial p}$ (GPa^{-1})	pressure range (GPa)	T (K)	Ref.
–0.029(3)	0–0.9	4.2	[101]
–0.017(2)	0–6.1	4.2	[96]
		method	
–0.006		LDA	this work
–0.007		PBE	this work
–0.009		WC	this work
–0.006		LDA + U_1	this work
–0.003		LDA + U_2	this work
–0.005		PBE + U_1	this work
0.000		PBE + U_2	this work
–0.004		B3PW91	this work

Table 9 Pressure dependence of the magnetic hyperfine field on Fe-IIa and Fe-IIb in γ′-Fe_4N (experiment and theory). $U_1 = 0.4$ eV, $U_2 = 1.8$ eV (Section 4).

$\frac{\partial \ln B_{IIa}}{\partial p}$ (GPa^{-1})	$\frac{\partial \ln B_{IIb}}{\partial p}$ (GPa^{-1})	pressure range (GPa)	T (K)	Ref.
–0.017(9)	–0.017(9)	0–0.9	4.2	[101]
–0.010(3)	–0.010(3)	0–6.1	4.2	[96]
			method	
–0.005	–0.005		LDA	this work
–0.005	+0.001		PBE	this work
–0.010	–0.003		WC	this work
–0.007	–0.002		LDA + U_1	this work
–0.002	+0.001		LDA + U_2	this work
–0.004	+0.000		PBE + U_1	this work
+0.002	+0.006		PBE + U_2	this work
–0.001	–0.006		B3PW91	this work

due the peculiar way in which the valence hyperfine field depends on the moment of the Fe neighbours.

From room temperature XMCD experiments under applied pressure, Ishimatsu et al. conclude that γ′-Fe_4N undergoes an isostructural phase transition to a paramagnetic phase at 24 GPa [95]. Ogura and Akai [114] have shown by full-potential KKR calculations what is the mechanism behind this transition: the Curie temperature drops with increasing pressure, and near 20 GPa it falls below room temperature. This implies that at 0 K, such a pressure-induced phase transition will not occur.

4 Computational details All new calculations reported here have been performed using state of the art *ab initio* methods within Density Functional Theory [16–18]. For solving the scalar-relativistic Kohn–Sham equations we have employed the Augmented Plane Waves + local orbitals (APW + lo) method [18, 115, 116] as implemented in the WIEN2k package [117]. In this method the wave functions are expanded in spherical harmonics inside nonoverlapping atomic spheres of radius R_{MT} and in plane waves in the remaining space of the unit cell (= the interstitial region). For calculations as a function of volume, we took $R_{MT}^{Fe} = 1.65$ a.u. and $R_{MT}^{N} = 1.45$ a.u. For final calculations at a given volume (as in Tables 1, 6, 10 and 11), those were $R_{MT}^{Fe} = 1.89$ a.u. and $R_{MT}^{N} = 1.67$ a.u. The maximum l for the expansion of the wave function in spherical harmonics inside the spheres was taken to be $l_{max} = 10$. The plane wave expansion of the wave function in the interstitial region was truncated at $K_{max} = 7.0/R_{MT}^{min} = (4.2–4.8)$ a.u.$^{-1}$, and the charge density was Fourier expanded up to $G_{max} = 12\sqrt{\text{Ry}}$. Local orbitals were added for the Fe-3s, Fe-3p and N-2s "semi-core" states. A mesh of 196 special k-points ($14 \times 14 \times 14$) in the irreducible Brillouin zone was used. Spin–orbit coupling was taken into account in all the calculations by a second variational step scheme [118] using a cutoff energy $E_{cut}^{SO} = 4.0$ Ry.

Several exchange-correlation functionals were used in this work: the Local Density Approximation (LDA) [15], the Perdew–Burke–Ernzerhof generalized gradient approximation (PBE) [77], the Wu–Cohen generalized gradient approximation (WC) [78], the LDA + U and PBE + U methods [119] to deal with enhanced electron correlations, and the hybrid B3PW91 functional [72, 86]. When using LDA + U or PBE + U, an important question is which value to take for the parameter U. The larger U, the stronger electron correlation effects are (see also Section 2.2). For instance, the correlated 3d electrons in the transition metal oxide Fe_3O_4 can be described with $U = 7.5$ eV [120], while stronger correlated 4f electrons require $U = 9.5$ eV [121]. LDA + U has been used abundantly for iron oxides, and it can be expected that LDA + U would improve the description of the less frequently studied iron nitrides as well [122, 123]. LDA + U has been used for the related $Fe_{16}N_2$ compound, with $U = 4$ eV [71]. The latter value was criticized in Ref. [34] as being too large for metallic transition metal nitrides. We addressed the choice of U in a pragmatic way by inspecting the total magnetization, the orbital moments, the magnetic hyperfine fields and the EFG as a function of U at the experimental lattice constant (Fig. 2). The total moment as well as the orbital moments increase with U, and the picture with the hyperfine information contains some clues to set reasonable values for U. For $U > 3$ eV, the EFG's at the Fe-IIa and Fe-IIb sites become noticeably different from each other, which is not in agreement with experiment. This excludes such large values of U, and confirms the argument in Ref. [34] about the excessively large $U = 4$ eV in Ref. [71] for iron-nitrides. With increasing U, the hyperfine field at Fe-I rapidly becomes larger than is acceptable when comparing to experiments. This criterium suggests a small value of U, and therefore we take $U = 0.4$ eV as our first trial value. All calculations with this U will be indicated as LDA + U_1 and PBE + U_1 throughout this paper.

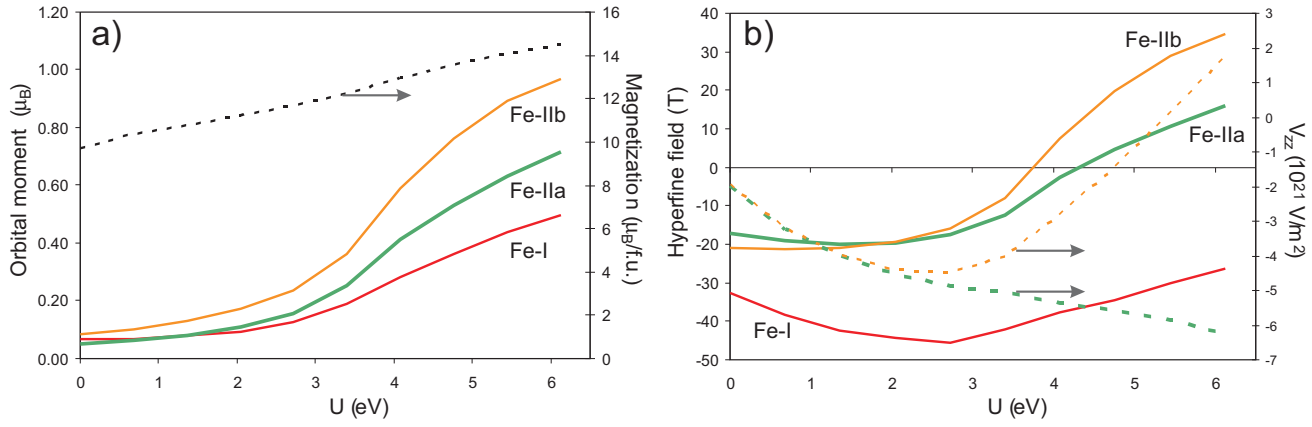

Figure 2 (online colour at: www.pss-b.com) (a) Orbital moments (left axis) for the three Fe-sites and saturation magnetization (right axis) as a function of U. (b) Magnetic hyperfine fields (left axis) and EFG's (right axis) as a function of U. The figure is for LDA + U at the experimental lattice constant. Results for PBE + U are very similar. The colour coding in both figures is as in Fig. 1.

Table 10 Spin and orbital moments for the three Fe-sites in γ′-Fe_4N, calculated with different exchange-correlation functionals at the experimental lattice constant and at the equilibrium lattice constant for each functional. The sum of these spin and orbital moments is the total moment reported in Table 1. $U_1 = 0.4$ eV, $U_2 = 1.8$ eV (Section 4).

		spin moment (μ_B)			orbital moment (μ_B)		
method	a_0 (Å)	Fe-I	Fe-IIa	Fe-IIb	Fe-I	Fe-IIa	Fe-IIb
LDA	3.790	2.84	2.12	2.12	0.07	0.05	0.08
PBE	3.790	2.88	2.30	2.30	0.06	0.05	0.08
WC	3.790	2.87	2.25	2.25	0.06	0.05	0.08
LDA + U_1	3.790	2.87	2.27	2.27	0.07	0.06	0.09
LDA + U_2	3.790	2.98	2.52	2.51	0.09	0.10	0.15
PBE + U_1	3.790	2.92	2.39	2.39	0.06	0.06	0.09
PBE + U_2	3.790	3.02	2.60	2.60	0.08	0.09	0.14
B3PW91	3.790	3.12	2.73	2.73	–0.01	–0.01	–0.03
LDA	3.629	2.73	1.16	1.16	0.05	0.00	0.02
PBE	3.790	2.84	2.27	2.32	0.06	0.05	0.08
WC	3.694	2.83	1.47	1.49	0.06	0.02	0.05
LDA + U_1	3.644	2.82	1.35	1.34	0.06	0.01	0.04
LDA + U_2	3.718	2.90	2.39	2.39	0.07	0.08	0.12
PBE + U_1	3.797	2.92	2.40	2.40	0.06	0.06	0.09
PBE + U_2	3.826	3.04	2.64	2.64	0.08	0.10	0.15
B3PW91	3.828	3.10	2.73	2.70	–0.01	–0.03	0.00

Experiments strongly suggest that the two hyperfine fields at the Fe-IIa and Fe-IIb sites are equal to each other. Although they are indeed close to each other in Fig. 2, they are equal only for $U = 1.8$ eV. This becomes therefore our second trial value, and these calculations will be labeled as LDA + U_2 and PBE + U_2.

Several quantities calculated in this paper are reported in tables and figures, and this for all 8 exchange-correlation functionals that were examined: structural properties (Table 4), saturation magnetization and atom-resolved moments (Table 1), magnetic hyperfine fields and EFG's (Table 6), spin and orbital contributions to the moments (Table 10), Fermi contact, orbital and spin dipolar contributions to the hyperfine field (Table 11), pressure dependence of the magnetization (Table 7) and of the hyperfine fields (Tables 8 and 9), saturation magnetization as a function of the lattice constant (Fig. 4), hyperfine parameters as a function of the saturation magnetization (Fig. 5) and hyperfine parameters as a function of the lattice constant (Fig. 6).

5 The best theoretical description For various properties (structural, magnetic and hyperfine properties, and pressure-dependencies), we will now discuss the (dis)agreement between experiment and the 8 different calculation methods that were described in Sections 4 and 2. Can we identify a method that gives the most satisfying description of γ′-Fe_4N?

5.1 Structural properties Table 4 gives the structural parameters that are determined from our calculated energy-versus-volume curves by a Birch–Murnaghan [97] fit in the volume range of ±10% around the minimum. LDA manifests its underbinding behaviour by providing the smallest of these lattice constants. The lattice constant by PBE is very close to the experimental value, and WC gives a result halfway LDA and PBE. Exactly the same trend as we see here for this transition metal nitride has been observed recently for the transition metal oxides MnO, FeO, CoO, NiO and ZnO [73]. When we turn to LDA + U/PBE + U, the equilibrium volume changes to larger values. $U = 0.4$ eV gives for LDA as well as for PBE a shift of 0.008 Å. $U = 1.8$ eV gives a shift of 0.08 Å for LDA and 0.04 Å for PBE. The hybrid B3PW91 functional has together with PBE + U_2 the largest lattice constant.

When zooming in on the details of the energy-versus-volume curves, it can be seen they are not completely smooth. This is illustrated for PBE + U_1 in Fig. 3. In all cases, there is a small kink that coincides with the sudden drop of the saturation magnetization that is plot in Fig. 3 as well. This has been pointed out first by Mohn and Matar [32] for LDA. Ogura and Akai [114] traced this back to a weakly pronounced double minimum in the moment/volume space, which leads to an almost continuous change from the high-spin to the low-spin minimum if the lattice constant is reduced. In order to have clean Birch–Murnaghan fit results in Table 4, we made sure to make the fit in a region around the minimum that does not contain the kink. For LDA, LDA + U_1 and WC we observe the minimum energy to be in the low-spin region. For the other 5 cases, the minimum has a high spin. As the high-spin solution has a somewhat larger lattice constant than the low-spin solution, this influences the trend in the calculated lattice constant: for WC, the two solutions have nearly the same energy, and the high-spin solution has almost the same lattice constant as for PBE. The larger volume increase for LDA + U_1 → LDA + U_2 than for PBE + U_1 → PBE + U_2 is due to the fact that in the former the kink in the moment curve jumps to the other side of the minimum.

In Fig. 3, the energy of the nonmagnetic solution for PBE is drawn as well. The ferromagnetic and nonmagnetic curves smoothly join and never cross, i.e. the ferromagnetic solution always has the lowest energy. The same is true for all other methods (not shown). This means that at 0 K pressure will not be able to induce a transition to the paramagnetic phase, which is consistent with experiment and with the conclusions obtained by Ogura and Akai [114] (see also Section 3.3).

The LDA-derived methods have the larger bulk modulus, while PBE(+ U), WC and B3PW91 all have a bulk modulus somewhat under 200 GPa. The bulk modulus becomes smaller with increasing U. There is no clear trend in the pressure derivative of the bulk modulus, all methods give a value around 5. When compared with the experimental values, LDA gives a bulk modulus that is clearly too large. The other methods give a bulk modulus that is still 50–60 GPa larger than the most reliable experimental

Table 11 Fermi contact, orbital and spin dipolar hyperfine fields (hff) (Tesla) for the three Fe-sites in γ′-Fe_4N, calculated with different exchange-correlation functionals at the experimental lattice constant and at the equilibrium lattice constant for each functional. The sum of these three contributions is the total hyperfine field reported in Table 1. U_1 = 0.4 eV, U_2 = 1.8 eV (Section 4).

method		Fermi contact hff			orbital hff			dipolar hff		
	a_0 (Å)	Fe-I	Fe-IIa	Fe-IIb	Fe-I	Fe-IIa	Fe-IIb	Fe-I	Fe-IIa	Fe-IIb
LDA	3.790	–36.8	–22.2	–22.2	4.1	2.9	5.2	0.0	2.0	–4.1
PBE	3.790	–39.4	–23.7	–23.7	3.4	2.9	5.0	0.0	1.7	–3.4
WC	3.790	–37.4	–22.6	–22.6	3.5	2.9	5.0	0.0	1.8	–3.7
LDA + U_1	3.790	–40.5	–23.5	–23.5	4.1	3.4	5.9	0.0	1.8	–3.6
LDA + U_2	3.790	–48.8	–27.5	–27.5	5.4	6.1	9.9	0.0	1.4	–2.7
PBE + U_1	3.790	–42.7	–25.0	–25.0	3.6	3.3	5.7	0.0	1.5	–3.1
PBE + U_2	3.790	–50.1	–28.5	–28.6	4.7	5.6	8.9	0.0	1.2	–2.2
B3PW91	3.790	–52.7	–31.0	–31.1	–1.5	–2.6	–1.0	–0.2	1.1	–2.4
LDA	3.629	–26.0	–18.1	–18.1	3.2	–0.5	0.7	0.0	2.6	–5.5
PBE	3.790	–39.6	–23.8	–23.8	3.4	2.8	4.9	0.0	1.7	–3.4
WC	3.694	–28.3	–22.1	–22.0	3.5	0.8	2.9	0.0	2.8	–6.0
LDA + U_1	3.644	–29.7	–21.0	–21.1	3.7	0.4	2.7	0.0	3.0	–6.3
LDA + U_2	3.718	–47.5	–26.5	–26.5	4.7	4.8	8.1	0.0	1.5	–3.0
PBE + U_1	3.797	–42.9	–24.9	–24.9	3.6	3.3	5.7	0.0	1.5	–3.0
PBE + U_2	3.826	–51.1	–28.6	–28.7	5.1	6.1	9.5	0.0	1.1	–1.9
B3PW91	3.828	–53.0	–31.4	–31.5	–1.3	–2.4	–0.6	–0.3	0.9	–2.1

value (141 GPa, see Section 3.1), which is not much regarding the sample dependence in the experimental value. We will put forward in Section 5.2 the hypothesis that in Nature a steep feature in the magnetization-versus-volume curve coincides with the equilibrium volume. This would considerably influence the bulk modulus, and can be the explanation for the remaining discrepancy between the bulk moduli in Table 4 and the experimental value.

When considering also the experimental values for the lattice constant, we can conclude that apart from the LDA-based methods, all functionals provide a reasonable description of the structural properties of γ′-Fe_4N. This is consistent with earlier studies for iron-mononitrides, where it was found that PBE gives a better description than LDA [124–126].

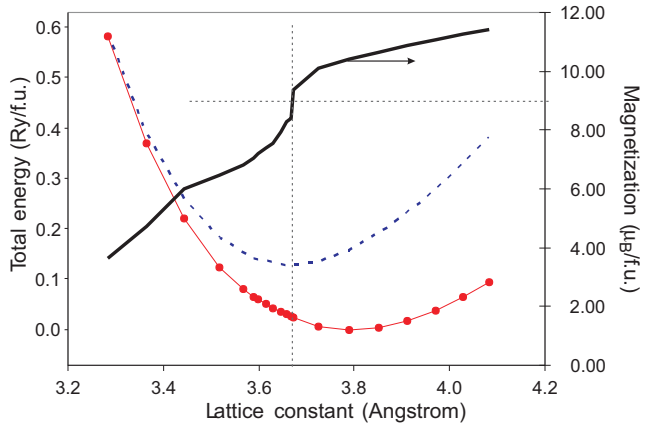

Figure 3 (online colour at: www.pss-b.com) Left axis: Total energy as a function of lattice constant for PBE + U_1, for the ferromagnetic (full line) and for the paramagnetic case (dashed line). Right axis: Saturation magnetization per formula unit (including orbital contributions) as a function of lattice constant. A kink in the total energy curve coincides with the steep feature in the magnetization curve. The horizontal and vertical dashed lines indicate the lattice constant that coincides with the experimental saturation magnetization.

5.2 Saturation magnetization Upon reducing the volume, the calculated saturation magnetization drops from a high value to zero in two distinct steps (Fig. 4). With increasing electron correlation (LDA → PBE → B3PW91, or with increasing U) the step moves to smaller volumes and the value of the magnetization at a given volume increases. This is reminiscent to what happens in Cr metal [127] for LDA and PBE, and illustrates the stronger magnetizing behaviour of gradient approximation functionals. Mohn and Matar [32] have shown that the drop at the highest volume is due to Fe-II only. The horizontal and vertical lines in Fig. 4 indicate the experimental value for the low-temperature saturation magnetization (≈9.0μ_B, Table 2) and the lattice constant, respectively. It can be seen from Fig. 4 and from Table 1 that at the experimental volume all methods overestimate the magnetization by more than 1μ_B/f.u. At the respective theoretical lattice constants this is still true, except for LDA, LDA + U_1 and WC which now strongly underestimate experiment: this is due to the fact that at that volume we are in the low-spin part of their magnetization curves. The magnetization by B3PW91 and by the U = 1.8 eV calculations is that high that we can rule them out as candidates for the best possible method to describe γ′-Fe_4N. Further arguments for this will be given in Section 5.3.

The consistent overestimation of the experimental magnetization is found by many other computational methods as well (Table 1, note that all calculations prior to

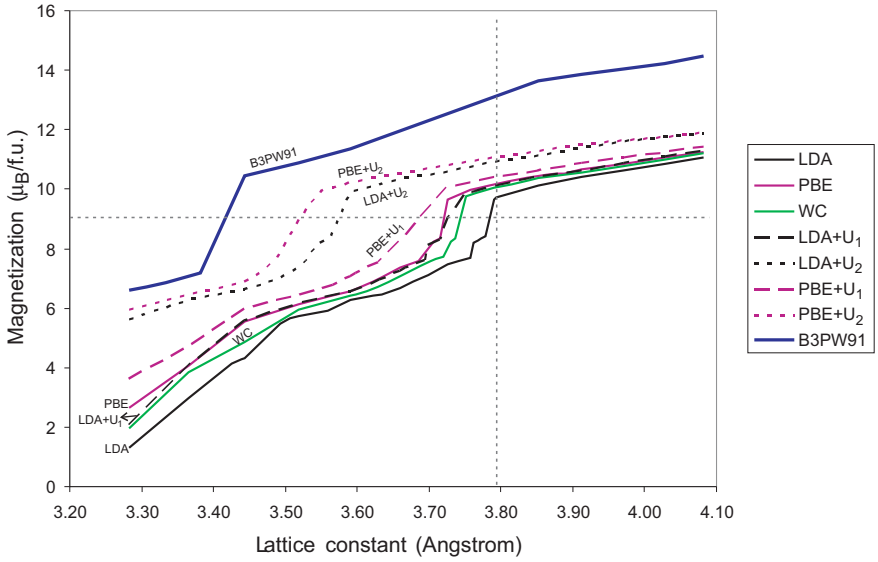

Figure 4 (online colour at: www.pss-b.com) Saturation magnetization as a function of lattice constant for 8 different exchange-correlation functionals. The horizontal dashed line indicates the low-temperature experimental saturation magnetization, the vertical dashed line the experimental lattice constant.

the present paper report the spin part of the magnetization only, without the orbital part). Such deviations are larger than usual for these functionals. Such an 'observation' – a functional that fails in situations where it is expected to perform well – is often an indication that something special is happening. Maybe the magnetic structure is not a simple ferromagnet, but something more complex that is experimentally not easily distinguished from a ferromagnet, yet yields a lower magnetization? We tested this hypothesis by calculating several 'nearly ferromagnetic' antiferromagnetic configurations (= a ferromagnetic supercell with the moment flipped over 180° for a small number of atoms), but these configurations were either unstable or had a larger total energy. The same was true for a series of non-collinear [128] configurations we tried. Another possibility – which is the hypothesis we will defend in the rest of the paper – is that *in Nature the equilibrium volume of* γ′-Fe_4N *coincides with the steep step in the magnetization-versus-volume curve*, more or less as it is the case for the WC functional. Small imperfections in the various functionals that usually would have minor consequences only, would then become much more prominent. If the equilibrium volume for a functional falls to the left of the magnetization step, then the predicted magnetization would be much too low. This is what happens for LDA, LDA + U_1 and WC. If if falls to the right of the step, then the magnetization is too large – this happens for other 5 functionals. Even if the equilibrium volume would fall at the position of the step, but not exactly at the right position, the predicted magnetization could still be considerably off.

A consequence of this hypothesis is that the saturation magnetization would be very strongly dependent on the volume, and therefore on the pressure. We will examine this consequence in Section 5.4, but first we will look at the predicted hyperfine information for the different functionals.

5.3 Hyperfine properties When comparing *ab initio* calculated hyperfine fields with experiment, some sources of possible deviations need to be taken into account. It is known [81, 82, 129, 130] that when using the common exchange-correlation functionals the contribution by the core electrons to the Fermi contact field is underestimated by about 4 $(T/\mu_B)\,\mu_{spin}$ [81] for 3d elements. For the present case, it would mean that the true contact hyperfine fields in Table 11 should be about 11 T (Fe-I) to 8 T (Fe-II) more negative. On the other hand, functionals without extra correlation effects underestimate the orbital moment and orbital hyperfine field, for Fe by roughly a factor 2 [80, 82]. This partly compensates the error in the contact contribution. Taken all together, a deviation of 5 T or a bit more between the most accurate calculations and experimental hyperfine fields is not uncommon, with the experimental values being somewhat more negative than the calculated ones. For EFG's, the rule of thumb is that a relative deviation of 10% for large field gradients and an absolute one of 1×10^{21} V/m^2 for small field gradients (as in the present case) is a typical error. When applying these two criteria to Table 6, we conclude that at the experimental lattice constant only the 5 weakly correlated functionals (LDA, PBE, WC, LDA + U_1 and PBE + U_1) give an acceptable description. At the respective theoretical lattice constants, only PBE and PBE + U_1 pass the test. The latter is due to the fact that the theoretical lattice constant for LDA, WC and LDA + U_1 falls at the low-spin side of the magnetization curve, which leads to magnetic hyperfine fields that are substantially too low. Arguments to dismiss LDA + U_2, PBE + U_2 and B3PW91 are a too large hyperfine field for Fe-I and/or a too large EFG. For B3PW91, the hyperfine field for Fe-II is too large as well.

An interesting way to summarize all hyperfine information is given in Fig. 5. It shows for all 8 functionals at the experimental and at the theoretical equilibrium lattice

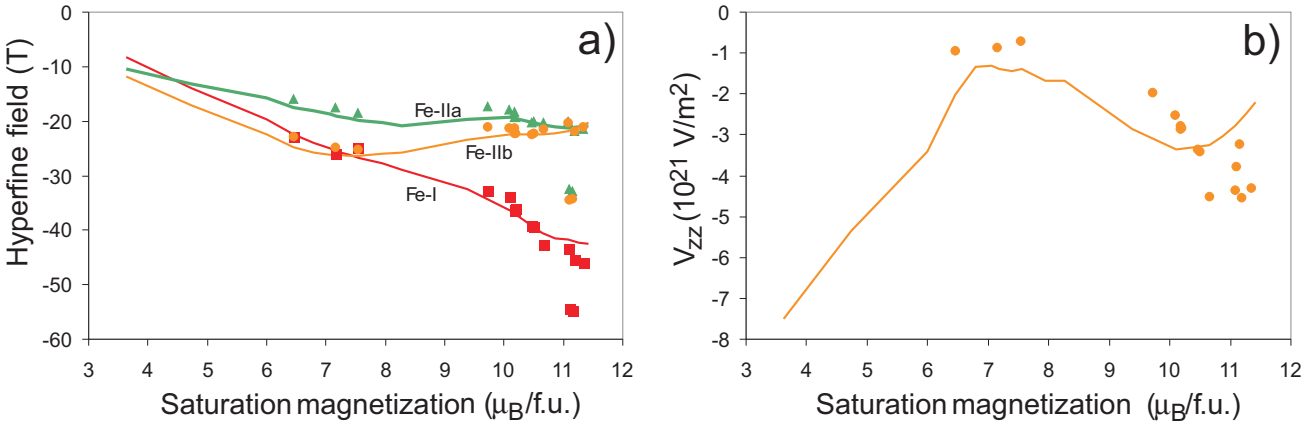

Figure 5 (online colour at: www.pss-b.com) (a) Hyperfine fields of the 3 Fe-sites as a function of the saturation magnetization, for 8 exchange-correlation functionals. Symbols: at the experimental or theoretical lattice constants. Lines: for PBE + U_1 (all lattice constants). (b) EFG as a function of the saturation magnetization. The colour coding is as in Fig. 1.

constant the hyperfine fields (Fig. 5a) and EFG (Fig. 5b) *as a function of the total magnetization* at those lattice constants. Superimposed on this is the same information for the PBE + U_1 functional, for all the studied lattice constants. There is a consistent trend visible in these pictures, which is broken only by B3PW91 (for which we by the above arguments do not expect it gives a reasonable description here anyway). This suggests that to a large extent the variation among the different functionals is due to differences in the magnetization-versus-volume curves (Fig. 4), which can be filtered away if the properties of interest are plot directly as a function of the magnetization. Therefore, we list in Table 12 the hyperfine fields and electric field gradients for all functionals at the lattice constant where the total magnetization is equal to the experimental value of 9.0(2)μ_B/f.u. The hyperfine fields by all functionals are rather similar (except for B3PW91), with a spread of less than 4 T for any site. The calculated values are up to a few Tesla less negative than the experimental ones, in agreement with the general trend (see the beginning of this section). The spread in the EFG is larger, and definitely the stronger correlated functionals provide a better field gradient than LDA, PBE or WC. This is consistent with our initial expectation that some degree of additional electron correlation should be present in iron nitrides. Among the former functionals, the EFG by PBE + U_1 (U = 0.4 eV) is very close to the experimental value.

According to the last column of Table 12, all functionals agree that at this magnetization there is a difference of about 4 T between the hyperfine fields at the Fe-IIa and Fe-IIb sites. This difference is also present in Fig. 5, from which it can be seen to disappear only at very large magnetization values. It does not originate from the Fermi contact fields, which are identical for both sites in all cases (–24.6 T for PBE + U_1). The reason for the difference lies in the orbital (2.4 T and 4.7 T for PBE + U_1) and dipolar (2.1 T and –4.4 T for PBE + U_1) contributions. The only two functionals that have equal Fe-II hyperfine fields are LDA + U_2 and PBE + U_1 at the experimental lattice constant, because the value of U was tuned to obtain this zero difference. But at the lattice constant that provides the experimental value for the magnetization, the difference is present for these functionals as well. The experimental values in Table 5, however, do not give any indication of

Table 12 Lattice constants a_0 (Å) and hyperfine properties B_{hf} and V_{zz} (T and 10^{21} V/m^2, respectively) for all examined functionals at the lattice constant where the magnetization per formula unit is equal to the experimental value of 9.0μ_B/f.u. The last column gives the difference between the hyperfine fields at the Fe-IIa and Fe-IIb sites. The line with experimental values is a summary of the low-temperature data from Table 5. U_1 = 0.4 eV, U_2 = 1.8 eV (Section 4).

functional	a_0 at 9.0μ_B	B_{hf}-I	B_{hf}-IIa	B_{hf}-IIb	V_{zz}^{IIa}	V_{zz}^{IIb}	(B_{hf}-IIa)–(B_{hf}-IIb)
LDA	3.786	–30.9	–18.4	–22.5	–1.2	–1.2	4.1
PBE	3.736	–29.6	–19.8	–23.9	–1.3	–1.3	4.1
WC	3.746	–29.2	–18.6	–23.0	–1.6	–1.6	4.4
LDA + U_1	3.726	–31.2	–19.4	–23.0	–1.8	–1.8	3.7
LDA+ U_2	3.572	–33.1	–20.1	–23.3	–3.4	–3.2	3.3
PBE+ U_1	3.668	–31.2	–20.1	–24.2	–2.4	–2.5	4.1
PBE+ U_2	3.519	–33.1	–22.0	–25.3	–4.2	–4.3	3.4
B3PW91	3.378	–24.4	–18.7	–17.7	–4.6	–5.2	–1.0
exp		–36.9	–23.6	–23.6	–2.7	–2.7	0.0

such a 4 T difference. We tried to reproduce published experimental Mössbauer spectra with a difference between the Fe-II hyperfine fields, but these attempts were unambiguously unsuccessful. This suggest that the reason for the disagreement is at the computational side, in particular in the calculation of the orbital and/or dipolar contributions to the hyperfine field. One possible explanation is that in the true ground state of Fe_4N the orbital occupation of the Fe atoms might be qualitatively different from the occupations provided by LDA or PBE – occupations which are used as the starting situation for the subsequent LDA + U and PBE + U calculations. A different orbital occupation would lead to different orbital and dipolar hyperfine fields. This has not been examined any further in the present work, but it has been shown before that LDA + U can stabilize qualitatively different orbital occupations in iron compounds [131] and in lanthanide [121] compounds.

5.4 Pressure dependence A comparison between the experimental and theoretical pressure dependencies of magnetization and hyperfine fields (Tables 7–9) shows that the experimental pressure dependence is considerably larger than the calculated dependence *near the theoretical lattice constants*. This holds for all 8 functionals. This can be recognized in Fig. 4 as well, where all the theoretical lattice constants fall in rather flat areas of the magnetization-versus-volume curves. If however, the lattice constant would coincide with the steep feature in those magnetization curves, the pressure dependence of the magnetization would be much larger. Interestingly enough, for *all* 8 functional the experimental value of the magnetization ($9.0\mu_B$/f.u.) falls in the range of this steep feature. If we now follow the same reasoning as for the hyperfine parameters (Section 5.3), and examine the pressure dependence of the magnetization *at the lattice constant that corresponds to the experimental magnetization*, we find values that are much larger and hence much closer to experiment. Quantifying this statement is not straightforward, as by the arbitrary act of identifying the zero pressure situation to the lattice constant at which the magnetization is $9.0\mu_B$ we cannot assign a value for the pressure to the other lattice constants. For the PBE + U_1 functional, we show the volume dependence of hyperfine fields and EFG in Fig. 6. The dashed line indicates the lattice constant that corresponds to the experimental magnetization, which coincides with a discrete jump in all hyperfine quantities (this holds for all other functionals as well). We did not perform Fixed Spin Moment calculations as in Ref. [114], and can therefore not completely exclude the possibility of a (small) hysteresis here. It can be readily seen from Fig. 6 that upon applying pressure the hyperfine fields of Fe-I and Fe-IIa decrease, while the one of Fe-IIb slightly increases. Given the unanimity of all functionals on this feature, and given the good description of a.o. the pressure dependence of the magnetization, this is a observation that cannot easily be put aside, even though experiment [107, 108] claims that the hyperfine fields at all Fe sites decrease. A further investigation of this issue seems worthwhile.

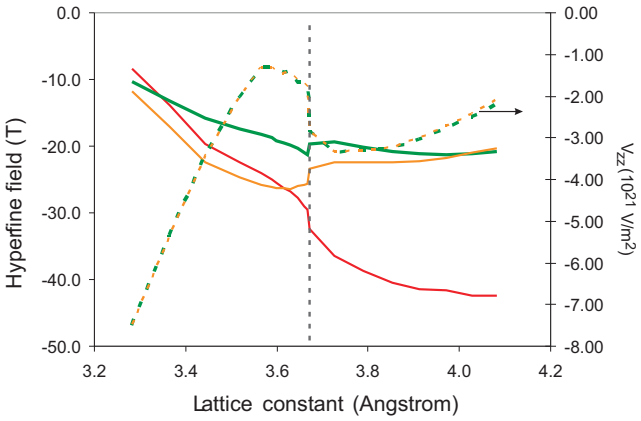

Figure 6 (online colour at: www.pss-b.com) Magnetic hyperfine fields for the Fe-I, Fe-IIa and Fe-IIb sites, and EFG's for the Fe-IIa and Fe-IIb sites, as a function of lattice constant (PBE + U_1). The vertical dashed line indicates the lattice constant at which the experimental value of the magnetization is reached. The colour coding is as in Fig. 1.

5.5 The best functional One of the goals of this paper was to identify the best currently available theoretical description of γ′-Fe_4N. From the arguments given earlier in this section, these are our conclusions:

The best prediction of structural properties is given by the gradient-corrected functionals. Lattice constants are nearly perfect, while uncertainties in the experimental values do not allow to determine how large the remaining discrepancy in the bulk modulus and its pressure derivative are. All 8 exchange-correlation functionals that were examined in this paper predict a steep feature in the magnetization-versus-volume curves (Fig. 4). The position of this feature relative to the theoretical lattice constant as well as relative to the experimental lattice constant is different for every functional. We put forward the hypothesis that in Nature this steep feature appears *precisely* at the experimental lattice constant. This explains in a natural way why all functionals give a magnetization that is considerably off, and it also provides the observed strong pressure dependence of the magnetization. All functionals give acceptable magnetic hyperfine fields at the experimental magnetization, but PBE + U_1 (U = 0.4 eV) gives the best EFG. We therefore propose PBE + U_1 as the best functional for structural properties (without restriction) as well as for magnetic, hyperfine and pressure-dependent properties (when tuned to the experimental magnetization). That a moderate amount of additional electron correlations is beneficial, is not a surprize for iron nitrides [34, 122, 123].

6 A high magnetization? As described in Section 1.1, an exceptionally large saturation magnetization of $11.6\mu_B$/f.u. was recently measured in γ′-Fe_4N [21]. Based on the consistent predictions of all 8 examined functionals,

with and without additional electron correlations, it seems very unlikely that this high value is an intrinsic property of γ′-Fe_4N. Let us therefore examine this experimental study more closely. An obvious reason why the magnetization could be anomalously large, is that the samples could contain not only Fe_4N, but also a second phase with a large moment. This happened for instance in the work of Ma et al. [66], where a large magnetization in Fe_4N/SiN multilayers annealed at 500 °C could be correlated with the appearance of α-Fe, as detected by XRD. The γ′-Fe_4N samples with high magnetization studied in Ref. [21] by Atiq et al. were grown and annealed at 450 °C, and their composition was inspected by XRD. For annealing times of 10, 20 and 30 minutes, the diffraction peaks due to γ′-Fe_4N grew stronger, and only at 40 minutes annealing α-Fe peaks appeared. Although this looks reassuring as far as sample quality is concerned, it does not prove that no α-Fe was present in the samples annealed for 30 minutes (those were the samples with the largest magnetization). It only proves that no *sufficiently large* crystallites of α-Fe (or another material) were present.

Even if a part of the increased magnetization would be due to α-Fe, it might not explain the entire observation. Indeed, even at only 10 minutes of annealing time, the Atiq sample on MgO has a magnetization of 9.3μ_B/f.u., which is already larger than in any room temperature measurement in the literature. At this short annealing time, the γ′-Fe_4N phase is not yet fully perfect, as its diffraction peaks still grow stronger when the annealing time is increased. And observable α-Fe peaks appear only after a 4 times longer annealing period. This either suggests that the observed moment is really intrinsic to γ′-Fe_4N, or that it is due to a second phase that is not α-Fe, that develops very early in the annealing period, and that was not detected in the XRD pattern. Atiq et al. attribute the increased magnetization to a smaller lattice mismatch between Fe_4N and the substrate. Their main argument for this is the increase of the magnetization with decreasing lattice mismatch (Table 2, last 3 lines). That argument is not fully convincing, for two reasons. First, Table 2 shows other experiments with the same MgO and $SrTiO_3$ substrates that have a magnetization of more than 2μ_B/f.u. smaller than in the Atiq measurements. This shows that apart from the lattice mismatch there must be another factor that plays a role. Second [132], Atiq et al. report that the (200) diffraction peak of Fe_4N lies always at 47.91°, irrespective of the substrate. This means that the lattice constant of γ′-Fe_4N is the same in all their samples.

A decisive test to see whether the large magnetization is intrinsic to Fe_4N or is due to another phase, would be a Mössbauer experiment on the same samples where the large magnetization was observed. Figure 5 suggests that for a sample with a saturation magnetization of 11.6μ_B/f.u. the hyperfine field of Fe-II would not be affected, but the hyperfine field of Fe-I would be 10 T larger than the values commonly observed (Table 5). Such a difference can be unambiguously determined from a Mössbauer or NMR experiment. Also the EFG would be almost twice as large as in the 'common' samples. Although we estimate it to be unlikely that such measurements will confirm this giant magnetization to be intrinsic to γ′-Fe_4N, it cannot be completely excluded that an as yet unspecified/uncontrolled parameter in the production procedure of the Atiq samples brings them to the high-spin side of the magnetization curve, without affecting the structural properties.

7 Conclusions and outlook We have argumented that PBE + U_l (U = 0.4 eV) is the best currently available functional for structural properties of γ′-Fe_4N (without tuning) as well as for its magnetic, hyperfine and pressure-dependent properties (when tuned to the experimental magnetization). We explained why we are not convinced by the recent experimental claim for a very large saturation magnetization in γ′-Fe_4N, and we suggest Mössbauer or NMR experiments on these particular samples to examine this further.

For testing some of the arguments we used in the present work, further experimental and theoretical studies would be useful. An independent and accurate determination of the bulk modulus and its pressure derivative would help to resolve the contradiction between the two presently available experiments, and would allow to better assess the quality of the structure predictions by the different functionals. A clear contradiction between our calculations and the experimental evidence, is the 4 T difference between the hyperfine fields at the Fe-IIa and Fe-IIb sites. We did not succeed in reproducing the experimental Mössbauer spectra with this constraint, which suggests the source of this deviation lies in the calculation of the orbital and dipolar contributions to the hyperfine field. Calculating these contributions with an independent *ab initio* code would be a useful check, as well as examining whether different orbital occupations would lead to hyperfine fields that are in agreement with experiment. All the functionals we examined predict an *increase* of the Fe-IIb hyperfine field with pressure. Verifying this claim with an independent *ab initio* code and/or revisiting the experimental determination of these hyperfine fields under pressure at low temperature would be interesting too.

We did not attempt to calculate Mössbauer isomer shifts for γ′-Fe_4N, because this quantity cannot be obtained from first principles as accurately as magnetic hyperfine fields and electric field gradients can be. Recently however, good progress has been achieved in this respect [133, 134], and a detailed theoretical study of the isomer shift and its pressure dependence in γ′-Fe_4N now becomes possible. A systematic experimental examination of the temperature dependence of the isomer shift and the uncommon temperature dependence of the EFG (Section 3.2) in the high-temperature region (Table 5) might reveal whether something is happening to the crystal structure in this temperature range.

Finally, we hope that the present insight in the successes and limitations of this set of exchange-correlations functionals for γ′-Fe_4N will pave the way for a more reli-

able quantitative modeling of other phases of the iron-nitrogen system (including vacancies), and of related materials as XFe_3N (X = a transition metal). An examination of the EFG as a function of U for those iron nitrides that do have Fe atoms at a non-cubic site would reveal whether there is indeed a single value of U (close to 0.4 eV) that allows for a consistent modeling of the entire iron-nitrogen system. A relevant general question is whether also for other iron-nitrides the steep feature in the magnetization coincides with the actual lattice constant, and whether this is by chance or rather due to an underlying driving mechanism.

Appendix: List of acronyms An alphabetical list of acronyms that are used in this paper is given in Table 13.

Table 13 Alphabetical list of acronyms.

APW + lo	augmented plane waves plus local orbitals
ASA	atomic sphere approximation
ASW	augmented spherical wave method
B3PW91	Becke–Perdew–Wang GGA-based hybrid functional
CVD	chemical vapour deposition
dc-MS	direct current magnetron sputtering
DFT	density functional theory
DVM-SCC	discrete variational method in the self-consistent charge approximation
EFG	electric-field gradient
FLAPW	full-potential linearized augmented plane wave method
FLASTO	full-potential linearized augmented slater type orbital method
FLMTO	full-potential linearized muffin tin orbital method
GGA	generalized gradient approximation
hff	hyperfine field
KKR	Korringa–Kohn–Rostoker method
LCAO	linear combination of atomic orbitals
LDA	local density approximation
LDA + U	local density approximation plus Hubbard U
LMTO	linearized muffin tin orbital method
MBE	molecular beam epitaxy
OP	orbital polarization
PBE	Perdew–Burke–Ernzerhof functional
PBE + U	Perdew–Burke–Ernzerhof functional plus Hubbard U
rf-MS	radio frequency magnetron sputtering
TB	tight binding method
WC	Wu–Cohen functional
XC	exchange-correlation
XMCD	X-ray magnetic circular dichroism

Acknowledgements This work was performed as a Joint Research Project in the framework of a cooperation between the *Ministerio de Ciencia, Tecnología e Innovación Productiva* (MINCyT) of Argentina and the *Fonds voor Wetenschappelijk Onderzoek – Vlaanderen* (FWO) of Flanders (Belgium). Other support came from research projects G.0447.05 and G.0191.08 of the FWO, from the Concerted Action of the K.U.Leuven (GOA/2004/02), the Centers of Excellence Programme of the K.U.Leuven (INPAC, EF/05/005), the Belgian Interuniversity Attraction Pole program (IAP P6/42), research grants PIP 5283 from *Consejo Nacional de Investigaciones Científicas y Técnicas* (CONICET, Argentina) and BID 1728 OC/AR PICT 38047 from *Agencia de Promoción Científica* (Anpcyt, Argentina). This research made use of VIC, the HPC infrastructure of the K.U.Leuven. The authors gratefully acknowledge helpful discussions with D. Boerma (Madrid), P. Novák (Prague), and G. Steinle-Neumann (Bayreuth).

References

[1] P. H. Emmett, S. B. Hendricks, and S. Brunauer, J. Am. Chem. Soc. **52**, 1456 (1930).
[2] H. Hägg, Z. Phys. Chem. B **8**, 455 (1930).
[3] K. H. Jack, Proc. R. Soc. Lond. A **195**, 34 (1948).
[4] H. Jacobs, D. Rechenbach, and U. Zachwieja, J. Alloys Compd. **227**, 10 (1995).
[5] B. C. Frazer, Phys. Rev. **112**, 751 (1958).
[6] C. Guillaud and H. Creveaux, Compt. Rend. Acad. Sci. (Paris) **222**, 1170 (1946).
[7] C. Zener, Phys. Rev. **85**, 324 (1952).
[8] G. W. Wiener and J. A. Berger, Trans. Am. Inst. Mining Metall. Eng., J. Met. **203**, 360 (1955).
[9] G. Shirane, W. J. Takei, and S. L. Ruby, Phys. Rev. **126**, 49 (1962).
[10] C. A. Kuhnen, R. S. de Figueiredo, V. Drago, and E. Z. da Silva, J. Magn. Magn. Mater. **111**, 95 (1992).
[11] Q. Qi, K. O'Donnell, E. Touchais, and J. M. D. Coey, Hyperfine Interact. **94**, 2067 (1994).
[12] J. C. Wood and A. J. Nozik, Phys. Rev. **4**, 2224 (1971).
[13] J. L. Costa-Krämer, D. M. Borsa, J. M. García-Martín, M. S. Martín-González, D. O. Boerma, and F. Briones, Phys. Rev. B **69**, 144402 (2004).
[14] O. Bartels and K. D. Becker, Z. Phys. Chem. **221**, 1509 (2007).
[15] J. P. Perdew and Y. Wang, Phys. Rev. B **45**, 13244 (1992).
[16] P. Hohenberg and W. Kohn, Phys. Rev. **136**, B864 (1964).
[17] W. Kohn and L. J. Sham, Phys. Rev. **140**, A1133 (1965).
[18] S. Cottenier, Density Functional Theory and the Family of (L)APW-methods: a step-by-step introduction (Instituut voor Kern- en Stralingsfysica, KULeuven, Belgium, 2002), ISBN 90-807215-1-4 (freely available from http://www.wien2k.at/reg_user/textbooks).
[19] J. Kanamori, Prog. Theor. Phys. Supp. **101**, 1 (1990).
[20] J. M. D. Coey and P. A. I. Smith, J. Magn. Magn. Mater. **200**, 405 (1999).
[21] S. Atiq, H. S. Ko, S. A. Siddiqi, and S. C. Shin, Appl. Phys. Lett. **92**, 222507 (2008).
[22] S. Matar, P. Mohn, G. Demazeau, and B. Siberchicot, J. Phys. (France) **49**, 1761 (1988).
[23] A. Sakuma, J. Phys. Soc. Jpn. **60**, 2007 (1991).
[24] A. Sakuma, J. Magn. Magn. Mater. **102**, 127 (1991).
[25] S. Ishida and K. Kitawatase, J. Magn. Magn. Mater. **104**–**107**, 1933 (1992).
[26] S. Ishida, K. Kitawatase, S. Fujii, and S. Asano, J. Phys.: Condens. Matter **4**, 765 (1992).
[27] R. Coehoorn, G. H. O. Daalderop, and H. J. F. Jansen, Phys. Rev. B **48**(6), 3830–3834 (1993).

[28] J. M. D. Coey, K. O'Donnell, Q. Qi, E. Touchais, and J. H. Jack, J. Phys.: Condens. Matter **6**, L23 (1994).
[29] C. Paduani and J. C. Krause, J. Magn. Magn. Mater. **138**, 109 (1994).
[30] Y. Kong, R. Zhou, and F. Li, Phys. Rev. B **54**(8), 5460–5465 (1996).
[31] Y. Kong, R. Zhou, and F. Li, J. Phys.: Condens. Matter **8**, 3829 (1996).
[32] P. Mohn and S. F. Matar, J. Magn. Magn. Mater. **191**, 234 (1999).
[33] M. Sifkovits, H. Smolinski, S. Hellwig, and W. Weber, J. Magn. Magn. Mater. **204**, 191 (1999).
[34] G. W. Fernando, R. E. Watson, M. Weinert, A. N. Kocharian, A. Ratnaweera, and K. Tennakone, Phys. Rev. B **61**, 375 (2000).
[35] Y. R. Jang, I. G. Kim, and J. I. Lee, J. Magn. Magn. Mater. **263**, 366 (2003).
[36] E. L. Peltzer y Blancá, J. Desimoni, and N. E. Christensen, Physica B **354**, 341 (2004).
[37] C. Navio, J. Alvarez, M. J. Capitan, D. Ecija, J. M. Gallego, F. Yndurain, and R. Miranda, Phys. Rev. B **75**, 125422 (2007).
[38] G. Demazeau, D. Andriamandroso, M. Pouchard, B. Tanguy, and P. Hagenmüller, Compt. Rend. Acad. Sci. (Paris), Ser. II **297**, 843 (1983).
[39] D. Andriamandroso, G. Demazeau, M. Pouchard, and P. Hagenmüller, J. Solid State Chem. **54**, 54 (1984).
[40] S. F. Matar, G. Demazeau, and B. Siberchicot, IEEE Trans. Magn. **26**, 60 (1990).
[41] D. M. Borsa, S. Grachev, C. Presura, and D. O. Boerma, Appl. Phys. Lett. **80**, 1823 (2002).
[42] K. R. Nikolaev, I. N. Krivorotov, E. D. Dahlberg, V. A. Vas'ko, S. Urazhdin, R. Loloee, and W. P. Pratt, Appl. Phys. Lett. **82**(25), 4534 (2003).
[43] S. Kokado, N. Fujima, K. Harigaya, H. Shimizu, and A. Sakuma, Phys. Rev. B **73**, 172410 (2006).
[44] K. Sunaga, M. Tsunoda, K. Komagaki, Y. Uehara, and M. Takahashi, J. Appl. Phys. **102**, 013917 (2007).
[45] T. K. Kim and M. Takahashi, Appl. Phys. Lett. **20**, 492 (1972).
[46] Y. Sugita, M. Mitsuoka, M. Komura, H. Hoshiya, Y. Kozono, and M. Hanazono, J. Appl. Phys. **70**, 597 (1991).
[47] Y. Sugita, H. Takahashi, M. Komuro, K. Mitsuoka, and A. Sakuma, J. Appl. Phys. **76**, 6637 (1994).
[48] M. Komura, H. Hoshiya, M. Mitsuoka, Y. Kozono, and M. Hanazono, J. Appl. Phys. **67**, 5126 (1990).
[49] Y. Sugita, H. Takahashi, M. Komuro, M. Igarashi, R. Imura, and T. Kambe, J. Appl. Phys. **79**, 5576 (1996).
[50] S. Okamoto, O. Kitakami, and Y. Shimada, J. Appl. Phys. **85**, 4952 (1999).
[51] J. M. D. Coey, J. Appl. Phys. **76**(10), 6632 (1994).
[52] A. Sakuma, J. Appl. Phys. **79**(8), 5570 (1996).
[53] J. Q. Xiao and C. L. Chien, Appl. Phys. Lett. **64**, 384 (1994).
[54] H. Chatbi, M. Vergnat, P. Bauer, and G. Marchal, Appl. Phys. Lett. **67**, 430 (1995).
[55] H. Jiang, Q. L. Wu, K. Tao, and H. D. Li, J. Appl. Phys. **78**, 3299 (1995).
[56] M. A. Brewer, K. M. Krishnan, and C. Ortiz, J. Appl. Phys. **79**, 5321 (1996).
[57] L. Guibin, L. Guoqing, L. Minkai, and L. Bangzhi, Surf. Coat. Technol. **96**, 34 (1997).
[58] N. Takahashi, Y. Toda, T. Nakamura, and T. Fujii, Jpn. J. Appl. Phys. **38**, 6031 (1999).
[59] T. Yamaguchi, M. Sakita, M. Nakamura, and T. Kobira, J. Magn. Magn. Mater. **215**, 529 (2000).
[60] D. M. Borsa, S. Grachev, and D. O. Boerma, Appl. Phys. Lett. **79**, 994 (2001).
[61] T. Takahashi, N. Takahashi, N. Tamura, T. Nakamura, M. Yoshioka, W. Inamic, and Y. Kawata, J. Mater. Chem. **11**, 3154 (2001).
[62] S. Grachev, D. M. Borsa, S. Vongtragool, and D. O. Boerma, Surf. Sci. **482–485**, 802 (2001).
[63] R. Loloee, K. R. Nikolaev, and W. P. Pratt, Appl. Phys. Lett. **82**(19), 3281 (2003).
[64] L. L. Wang, W. T. Z. X. Wanga, N. Maa, Q. F. Guana, J. Zhaoa, Y. Chena, and S. Feng, Mater. Chem. Phys. **100**, 304 (2006).
[65] J. E. Mattson, C. D. Potter, M. J. Conover, C. H. Sowers, and S. D. Bader, Phys. Rev. B **55**(1), 70–73 (1997).
[66] N. Ma, X. Wang, W. T. Zheng, L. L. Wang, M. W. Wang, P. J. Cao, and X. C. Ma, Appl. Surf. Sci. **254**, 4786 (2008).
[67] R. J. Arnott and A. Wold, J. Phys. Chem. Solids **15**, 152 (1960).
[68] Y. D. Zhang, J. I. Budnick, W. A. Hines, M. Q. Huang, and W. E. Wallace, Phys. Rev. B **54**(1), 51–54 (1996).
[69] L. Wang, W. Zheng, J. Gong, H. Li, X. Wang, N. Ma, P. Cao, and X. Ma, J. Alloys Compd. **467**(1–2), 1–5 (2009).
[70] R. N. Panda and N. S. Gajbhiye, IEEE Trans. Magn. **34**, 542 (1998).
[71] W. Y. Lai, Q. Q. Zheng, and W. Y. Hu, J. Phys.: Condens. Matter **6**, L259 (1994).
[72] F. Tran, P. Blaha, K. Schwarz, and P. Novák, Phys. Rev. B **74**, 155108 (2006).
[73] F. Tran, R. Laskowski, P. Blaha, and K. Schwarz, Phys. Rev. B **75**, 115131 (2007).
[74] G. Zhang and C. B. Musgrave, J. Phys. Chem. A **111**, 1554 (2007).
[75] J. Hafner, J. Comput. Chem. **29**, 2044 (2008).
[76] D. M. Ceperley and B. J. Alder, Phys. Rev. Lett. **45**(7), 566–569 (1980).
[77] J. P. Perdew, K. Burke, and M. Ernzerhof, Phys. Rev. Lett. **77**, 3865 (1996).
[78] Z. Wu and R. Cohen, Phys. Rev. B **75**, 235116 (2006).
[79] P. E. A. Turchi, I. A. Abrikosov, B. Burton, S. G. Fries, G. Grimvall, L. Kaufman, P. Korzhavyi, V. R. Manga, M. Ohno, A. Pisch, A. Scott, and W. Zhang, Comput. Coupling Phase Diagrams Thermochem. **31**, 4 (2007).
[80] O. Hjortstam, J. Trygg, J. M. Wills, B. Johansson, and O. Eriksson, Phys. Rev. B **53**, 9204 (1996).
[81] R. Coehoorn, J. Magn. Magn. Mater. **159**, 55 (1996).
[82] P. Novák, J. Kunes, W. E. Pickett, W. Ku, and F. R. Wagner, Phys. Rev. B **67**, 140403(R) (2003).
[83] M. Brooks, Physica B **130**, 6 (1985).
[84] O. Eriksson, B. Johansson, and M. Brooks, J. Phys.: Condens. Matter **1**, 4005 (1989).
[85] F. Tran, J. Schweifer, P. Blaha, K. Schwarz, and P. Novák, Phys. Rev. B **77**, 085123 (2008).
[86] A. D. Becke, J. Chem. Phys. **98**, 5648 (1993).

[87] P. J. Stephens, F. J. Devlin, C. F. Chabalowski, and M. J. Frisch, J. Phys. Chem. **98**, 11623 (1994).
[88] F. Corà, M. Alfredsson, G. Mallia, D. S. Middlemiss, W. C. Mackrodt, R. Dovesi, and R. Orlando, Struct. Bonding **113**, 171 (2004).
[89] D. Torumba, P. Novák, and S. Cottenier, Phys. Rev. B **77**, 155101 (2008).
[90] J. Perdew, M. Ernzerhof, and K. Burke, J. Chem. Phys. **105**, 9982 (1996).
[91] K. N. Kudin, G. E. Scuseria, and R. L. Martin, Phys. Rev. Lett. **89**, 266402 (2002).
[92] J. Heyd, G. Scuseria, and M. Ernzerhof, J. Chem. Phys. **118**, 8207 (2003).
[93] J. Paier, M. Marsman, and G. Kresse, J. Chem. Phys. **127**, 024103 (2007).
[94] R. M. Martin, Electronic Structure: Basic Theory and Practical Methods (Cambridge University Press, 2004).
[95] N. Ishimatsu, H. Maruyama, N. Kawamura, M. Suzuki, Y. Ohishi, M. Ito, S. Nasu, T. Kawakami, and O. Shimomura, J. Phys. Soc. Jpn. **72**, 2372 (2003).
[96] C. L. Yang, M. M. Abd-Elmeguid, H. Micklitz, G. Michels, J. W. Otto, Y. Kong, D. S. Xue, and F. S. Li, J. Magn. Magn. Mater. **151**, L19 (1995).
[97] F. Birch, Phys. Rev. **71**(11), 809–824 (1947).
[98] P. Dufek, P. Blaha, and K. Schwarz, Phys. Rev. Lett. **75**, 3545 (1995).
[99] Y. Jirásková, S. Havlíčeka, O. Schneeweiss, V. Peřina, and C. Blawert, J. Magn. Magn. Mater. **234**, 477 (2001).
[100] D. Torumba, K. Parlinski, M. Rots, and S. Cottenier, Phys. Rev. B **74**, 144304 (2006).
[101] J. S. Lord, J. G. M. Armitage, P. C. Riedi, S. F. Matar, and G. Demazeau, J. Phys.: Condens. Matter **6**, 1779 (1994).
[102] A. Pösinger, J. Bogner, W. Steiner, P. Mohn, K. Schwarz, S. Matar, and G. Demazeau, Hyperfine Interact. **94**, 2093 (1994).
[103] A. J. Nozik, J. C. Wood, and G. Haacke, Solid State Commun. **7**, 1677 (1969).
[104] P. Rochegude and J. Foct, Phys. Status Solidi A **98**, 51 (1986).
[105] M. J. Clauser, Solid State Commun. **8**, 781 (1970).
[106] R. S. Figueiredo and V. Drago, Solid State Commun. **80**, 757 (1991).
[107] F. Li, Y. Kong, R. Zhou, C. L. Yang, M. M. Abd-Elmeiguid, G. Mkhels, H. Micklitz, and J. W. Otto, Solid State Commun. **95**, 753 (1995).
[108] F. S. Li and R. J. Zhou, J. Phys.: Condens. Matter **7**, L235 (1995).
[109] P. Schaaf, Hyperfine Interact. **111**, 113 (1998).
[110] Z. J. Zhao, D. S. Xue, and F. S. Li, J. Magn. Magn. Mater. **232**, 155 (2001).
[111] E. J. Miola, S. D. de Souza, and M. Olzon-Dionysio, Surf. Coat. Technol. **167**, 33 (2003).
[112] A. N. Timoshevskii, V. A. Timoshevskii, B. Z. Yanchitsky, and V. A. Yavna, Comput. Mater. Sci. **22**, 99 (2001).
[113] J. B. Yang, D. S. Xue, R. J. Zhou, and F. S. Li, Phys. Status Solidi A **153**, 307 (1996).
[114] M. Ogura and H. Akai, Hyperfine Interact. **158**, 19 (2004).
[115] E. Sjöstedt, L. Nordström, and D. J. Singh, Solid State Commun. **114**, 15 (2000).
[116] G. K. H. Madsen, P. Blaha, K. Schwarz, E. Sjöstedt, and L. Nordström, Phys. Rev. B **64**, 195134 (2001).
[117] P. Blaha, K. Schwarz, G. Madsen, D. Kvasnicka, and J. Luitz, WIEN2k, An Augmented Plane Wave + Local Orbitals Program for Calculating Crystal Properties (Karlheinz Schwarz, Techn. Universität Wien, Austria, 1999), ISBN 3-9501031-1-2.
[118] D. D. Koelling and B. N. Harmon, J. Phys. C **10**, 3107 (1977).
[119] V. I. Anisimov, I. V. Solovyev, M. A. Korotin, M. T. Czyżyk, and G. A. Sawatzky, Phys. Rev. B **48**(23), 16929–16934 (1993).
[120] G. K. H. Madsen and P. Novák, Europhys. Lett. **69**, 777 (2005).
[121] D. Torumba, V. Vanhoof, M. Rots, and S. Cottenier, Phys. Rev. B **74**, 014409 (2006).
[122] P. Novák and F. R. Wagner, Phys. Rev. B **66**(18), 184434 (2002).
[123] A. Janotti, D. Segev, and C. G. V. de Walle, Phys. Rev. B **74**, 045202 (2006).
[124] H. Shimizu, M. Shirai, and N. Zuzuki, J. Phys. Soc. Jpn. **67**, 922 (1998).
[125] Y. Kong, J. Phys.: Condens. Matter **12**, 4161 (2000).
[126] A. Houari, S. F. Matar, M. A. Belkhir, and M. Nakhl, Phys. Rev. B **75**, 064420 (2007).
[127] S. Cottenier, B. D. Vries, J. Meersschaut, and M. Rots, J. Phys.: Condens. Matter **14**, 3275 (2002).
[128] R. Laskowski, G. K. H. Madsen, P. Blaha, and K. Schwarz, Phys. Rev. B **69**, R140408 (2004).
[129] S. Blügel, H. Akai, R. Zeller, and P. H. Dederichs, Phys. Rev. B **35**(7), 3271–3283 (1987).
[130] L. Severin, M. Richter, and L. Steinbeck, Phys. Rev. B **55**(15), 9211–9214 (1997).
[131] J. Kuneš, H. Rosner, D. Kasinathan, C. O. Rodriguez, and W. E. Pickett, Phys. Rev. B **68**(11), 115101 (2003).
[132] Argument by D. Boerma (private communication).
[133] M. Filatov, J. Chem. Phys. **127**(8), 084101 (2007).
[134] R. Kurian and M. Filatov, J. Chem. Theory Comput. **4**, 278 (2008).
[135] D. Ecija, E. Jimenez, J. Camarero, J. M. Gallego, J. Vogel, N. Mikuszeit, N. Sacristán, and R. Miranda, J. Magn. Magn. Mater. **316**, 321–324 (2007).

